RANKL blockade inhibits cancer growth through reversing the tolerogenic profile of tumor-infiltrating (plasmacytoid) dendritic cells

Charlotte Pilard,[1] Patrick Roncarati,[1] Marie Ancion,[1] Margaux Luyckx,[1] Michael Renard,[1] Celia Reynders,[1] Thomas Lerho,[1] Florian Poulain,[1] Diane Bruyere,[1] Alizee Lebeau,[1] Elodie Hendrick,[1] Rebekah Crake,[2] Raphael Peiffer,[3] Marie-Julie Nokin,[2] Olivier Peulen,[3] Philippe Delvenne,[1,4] Pascale Hubert ●,[1] Michael Herfs ●[1]

[1]Laboratory of Experimental Pathology, GIGA-Cancer, University of Liege, Liege, Belgium
[2]Laboratory of Tumor and Development Biology, GIGA-Cancer, University of Liege, Liege, Belgium
[3]Metastasis Research Laboratory, GIGA-Cancer, University of Liege, Liege, Belgium
[4]Department of Pathology, University Hospital Center of Liege, Liege, Belgium

Correspondence to
Dr Michael Herfs;
M.Herfs@uliege.be

ABSTRACT

Background Originally identified for its involvement in bone remodeling, accumulating data emerged in the past years indicating that receptor activator of nuclear factor κB ligand (RANKL) actually acts as a multifunctional soluble molecule that influences various physiological and pathological processes. Regarding its role in carcinogenesis, while direct effects on tumor cell behavior have been precisely characterized, the impact of the RANKL/RANK system (and its inhibition) on the intratumoral immune landscape remains unclear.

Methods After various in silico/in situ/in vitro analyses, the immunotherapeutic efficacy of RANKL blockade (alone and in combination with immune checkpoint inhibitors (anti-programmed cell death protein-1 (PD-1)) or doxorubicin/paclitaxel-based chemotherapy) was investigated using different syngeneic mouse models of triple-negative breast cancer (4T1, 67NR and E0771). Isolated from retrieved tumors, 14 immune cell (sub) populations, along with the activation status of antigen-presenting cells, were thoroughly analyzed in each condition. Finally, the impact of RANKL on the functionality of both dendritic cells (DC) and plasmacytoid dendritic cells (pDC) was determined.

Results A drastic tumor growth inhibition was reproductively observed following RANKL inhibition. Strikingly, this antitumor activity was not detected in immunocompromised mice, demonstrating its dependence on the adaptive immune responses and justifying the diverse enriched signatures linked to immune cell regulation/differentiation detected in RANKL[high]-expressing human neoplasms. Interestingly, neoadjuvant chemotherapy (but not PD-1 checkpoint inhibition) potentiated the anticancer effects of RANKL blockade by priming effector T cells and increasing their infiltration within the tumor microenvironment. Mechanistically, we highlighted that RANKL indirectly promotes regulatory T cell differentiation and suppressive function by inhibiting the mTOR signaling pathway on antigen-presenting cells.

Conclusions Taken together, this study provides insight into the role of RANKL/RANK axis in immune tolerance, demonstrates the significant impact of RANKL-dependent

WHAT IS ALREADY KNOWN ON THIS TOPIC

⇒ Initially identified for its role in regulating bone formation, it is now widely recognized that the receptor activator of nuclear factor κB ligand (RANKL)/RANK axis extends its function far beyond bone biology. In cancer progression and metastasis, while the direct influence on malignant cell behavior has been well characterized, the impact of the RANKL/RANK ligand–receptor pair (and its inhibition) on tumor immune microenvironment remains largely unclear.

WHAT THIS STUDY ADDS

⇒ Not seen when immunocompromised mice were used, a substantial reduction of tumor growth (further amplified by neoadjuvant chemotherapy, but not by programmed cell death protein-1 checkpoint inhibition) was consistently detected in various syngeneic mouse models of triple-negative breast cancer following RANKL blockade. Mechanistically, in vivo/in vitro data revealed that RANKL acts as a tolerogenic signal on antigen-presenting cells (dendritic cells (DC)/plasmacytoid DC) through inhibiting the mTOR signaling pathway.

HOW THIS STUDY MIGHT AFFECT RESEARCH, PRACTICE OR POLICY

⇒ The findings collected in this study support that RANKL could be an interesting actionable target for cancer immunotherapy and emphasize the crucial role of the intratumoral immune landscape in the therapeutic efficacy of its blockade.

impairment of T cell–DC/pDC crosstalk on tumor development and, ultimately, supports that this ligand could be an interesting actionable target for cancer immunotherapy.

INTRODUCTION

Discovered simultaneously by several groups 25 years ago,[1–4] receptor activator of nuclear

factor κB ligand (RANKL) has also been initially defined as tumor necrosis factor-related activation-induced cytokine, osteoprotegerin (OPG) ligand or osteoclast differentiation factor before the recommendation of a standard nomenclature by the American Society for Bone and Mineral Research in 2000.[5] Highly conserved between species, RANKL is a transmembrane protein which can be cleaved by many metalloproteinases (eg, ADAM10 and 17, MMP3, 7 and 14), resulting in the formation of a soluble form acting well beyond its crucial activity in bone tissue remodeling (for a Review, see study by Ono et al[6]). Indeed, the RANKL/RANK axis has been shown to be involved in mammary gland development and lactation,[7] lymph node organogenesis[8] as well as in cancer progression/metastasis through favoring epithelial–mesenchymal transition and, possibly, immune tolerance/suppression (via an upregulation of CCL17 by macrophages and associated chemotaxis of T regulatory (Treg) cells in tumor microenvironment).[9] [10] Altogether, the accumulation of preclinical findings paved the way to many clinical trials assessing the potential anticancer properties of denosumab, an anti-RANKL monoclonal antibody used to treat osteoporosis in women at high risk for fracture. Aimed at determining the activity and safety of RANKL blockade alone as well as in combination with chemotherapeutic agents or anti-programmed cell death protein-1 (PD-1)/cytotoxic T-lymphocytes-associated protein 4 (CTLA-4) inhibitors, most of these multicenter phase II/III trials conducted in the context of various neoplasms (melanoma (NCT03161756), multiple myeloma (NCT03792763), clear cell renal carcinoma (NCT03280667), osteosarcoma (NCT02470091), nasopharyngeal carcinoma (NCT03923842),…) are still ongoing and the results are expected in the next few years. It is, however, important to mention that, despite a good tolerance, the first completed studies reported quite disappointing data and no bone metastasis-free survival improvement for denosumab-treated patients with breast/lung cancer (NCT01077154 and NCT02129699).[11] [12]

Breast cancer represents a relatively diverse group of malignancies affecting approximately one in eight women during her lifetime.[13] Supported by seminal gene expression profile analyses published in the early 2000s,[14] [15] the histological classification (eg, ductal, lobular,…) of breast neoplasms was successfully replaced by a molecular one (for which an immunohistochemistry-based surrogate is commonly preferred in daily practice).[16] Better reflecting the various disease mechanisms, treatment options and patient outcomes, three major subtypes (Luminal, human epidermal growth factor receptor 2+ (HER2+) and basal-like) have been consequently defined. Highly heterogeneous and associated with a poor prognosis, basal-like tumors do not generally express hormone (estrogen and progesterone) receptors and HER2; thereby, most of these latter are also commonly called triple-negative breast cancer (TNBC). Aimed at finding alternatives to the suboptimal cytotoxic anthracycline/taxane-based

chemotherapy as first-line treatment, both genomic and transcriptomic landscapes of TNBC have been precisely characterized, leading to the further division of this class of aggressive tumors (accounting for~15% of all breast cancers) into six (and then four) subclasses, each with putative therapeutic targets and biomarkers.[17–19] Inspired by these valuable findings, the field has been continuing to advance rapidly. Multiple clinical trials were conducted (or are still ongoing) and new drugs or combination therapies have recently been approved by the Food and Drug Administration (eg, olaparib (an oral PARP inhibitor) for the adjuvant treatment of BRCA1/2-mutated cancers, atezolizumab (anti-programmed death-ligand 1 (PD-L1 antibody) or pembrolizumab (anti-PD-1) plus chemotherapy for locally advanced or metastatic cancers,…),[20–22] bringing hope for patients with TNBC.

While most studies available in the literature have focused their attention on the direct effect of RANKL on epithelial tumor cells, using single-cell transcriptomic data, we first highlighted that other cancer-infiltrating cell types (especially immune cells) also express the receptor RANK (and could, therefore, be influenced by the RANKL/RANK axis as well). Supporting this hypothesis, more than half of the Top 10 Gene Ontology (GO) biological process gene sets enriched positively in RANKL[high]-expressing TNBC (an appropriate cancer (sub)type to analyze the potential therapeutic efficacy of RANKL blockade) were related to immune regulation/differentiation. Using different orthotopic, syngeneic TNBC models (4T1, 67NR, E0771), we then reported significant inhibitions of tumor growth (further enhanced by neoadjuvant chemotherapy) after a latency period of 5–7 days following the first injection of RANKL inhibitors, corresponding to the required time for the adaptive immunity to be remobilized. In agreement with this assumption (and the profound remodeling of the tumor immune microenvironment detected after RANKL blockade), the dependence on the adaptive immune system was clearly illustrated by the absence of therapeutic antitumor effect in immunocompromised mice. Using various in vitro assays, we finally showed that RANKL indirectly promotes regulatory T cell differentiation and suppressive function by acting as a tolerogenic signal on antigen-presenting cells. Mechanistically, this RANKL-induced immune defect, observed both in vitro and in vivo, was found to be linked to mTOR pathway inhibition.

MATERIALS AND METHODS
Tissue specimens
A total of 209 paraffin-embedded samples of invasive breast cancer (38 luminal A, 40 luminal B, 49 HER2+ and 82 TNBC (primary tumors, n=56; lung metastasis, n=26)) were retrieved from the Tissue Biobank of the University Hospital of Liege (Belgium) with the approval of the local ethics committee. Re-examined by experienced pathologists before subsequent immunohistochemical analysis,

all these tissue samples included both neoplastic areas and normal (healthy) epithelial cells.

Human/mouse cell lines and culture conditions

Kindly provided by Dr Nathalie Bendriss-Vermare (INSERM U1052/CNRS 5286, Claude Bernard Lyon 1 University, France), by Professor Hartmut Beug (University of Vienna, Austria), by Dr Sylvie Legrand-Poels (GIGA Inflammation, Infection and Immunity, University of Liege, Belgium) or purchased from CH3 BioSystems (Amherst, New York, USA), 1 macrophage-like (RAW264.7) and 7 mouse breast cancer (HER2+: Neu15; TNBC: 4T07, 4T1, 67NR, EpRas, EpH4, E0771) cell lines were used in this study and cultured at 37°C in a humidified CO_2 atmosphere until a 60–70% confluence was reached. Originally obtained from the American Type Culture Collection (Manassas, Virginia, USA), 10 human breast cancer cell lines (Luminal A: MCF7, T-47D; HER2+: SK-BR-3; TNBC: MDA-MB-157, MDA-MB-231, MDA-MB-468, BT-549, HCC70, HCC1143, Hs578T) as well as normal human mammary epithelial cells (MCF10A) were grown in Dulbecco's modified Eagle's medium (DMEM) or Roswell Park Memorial Institute (RPMI) 1640 medium (Gibco, Thermo Fisher Scientific, Waltham, Massachusetts, USA) supplemented with 10% fetal calf serum and various additives. Exact cell culture conditions are detailed in online supplemental table 1. All cell lines were invariably tested negative for mycoplasma contamination (MycoAlert Mycoplasma Detection Kit (Lonza, Verviers, Belgium)) throughout the present study.

Primary immune cell cultures

As previously described in detail,[23–25] both dendritic cells (DC) and plasmacytoid DC (pDC) were generated from CD34+ hematopoietic progenitor cells isolated from umbilical cord blood using the MACS CD34 MicroBead kit (Miltenyi Biotec, Bergisch Gladbach, Germany). Briefly, for the production of DC, CD34+ cells were cultured in the presence of human SCF (20 ng/mL, PeproTech, Cranbury, New Jersey, USA), TPO (10 ng/mL, PeproTech), Flt3L (25 ng/mL, PeproTech), GM-CSF (200 U/mL, Amoytop Biotech, Xiamen, China) and IL-4 (100 U/mL, ImmunoTools, Friesoythe, Germany) for 7 days. For the generation of large numbers of pDC with functional activities, CD34+ precursor cells were cultured in RPMI medium supplemented with 10% fetal calf serum, mercaptoethanol (50 µM, Gibco), TPO (10 ng/mL, PeproTech), Flt3L (100 ng/mL, PeproTech) and IL-3 (20 ng/mL, PeproTech) for 21 days. Where indicated, DC and pDC were incubated either with recombinant human RANKL (0.5 µg/mL, ab256098, Abcam, Cambridge, UK) for 3 days or with a mTOR inhibitor (Rapamycin (100 nM, Sigma-Aldrich, Saint Louis, Missouri, USA), Torkinib/PP242 (100 nM, Selleckchem, Houston, Texas, USA)) for 2 hours, followed by lipopolysaccharide (LPS) (1 µg/mL, Sigma-Aldrich) (for DC) or CpG ODN (12 µg/mL, Eurogentec, Seraing, Belgium) (for pDC)-induced maturation for 24 hours. DC/pDC phenotype (maturation markers: CD80, CD83, CD86, MHC class I/II and CCR7; inhibitory markers: ILT3 and ICOSL) was finally assessed using a FACSCanto II flow cytometer (GIGA in vitro imaging platform). All used fluorochrome-conjugated anti-human antibodies are listed in online supplemental table 2. The gating strategy is shown in online supplemental figure 1.

T cell–DC co-culture

Isolated from blood buffy coat using the MACS CD4 MicroBead kit (Miltenyi Biotec), CD4+ T cells were mixed with DC (generated as described above and pretreated or not with 0.5 µg/mL RANKL for 3 days) at a 10:1 ratio in 6-well plates. The medium for these co-culture experiments was constituted of RPMI 1640 supplemented with 5% human pooled AB serum. At day 6, CD4+ T cells were sorted before quantitative reverse transcription PCR (RT-qPCR) analysis.

T-cell suppression assay

A first mixed lymphocyte reaction (MLR) was performed using allogeneic CD4+ T cells purified from peripheral blood using the human CD4 T cell isolation kit (Miltenyi Biotec) and then co-cultured for 6 days with DC (generated as described above and pretreated or not with 0.5 µg/mL RANKL for 3 days before stimulation with 1 µg/mL LPS). The ratio between responder (lymphocytes) and effector (DC) cells was 10:1. In parallel, a second (control) MLR was performed using other allogeneic T cells and DC at a 10:1 ratio. Cell mixtures from the first MLR (and considered as potential "suppressor" cells) were then added at a 1:10 or 1:1 ratio corresponding to 1 "suppressor" cell for 10 or 1 responder cell(s). After 6 days of culture, cell viability/proliferation was assessed by MTT assay (Roche, Basel, Switzerland).

Cytokine array

Cytokines/chemokines secreted by DC incubated or not with 0.5 µg/mL RANKL for 3 days were detected using the Proteome Profiler array (R&D Systems, Minneapolis, Minnesota, USA), according to manufacturer's recommendations. For both conditions, cell culture supernatants (2×10^6 DC per well in a 6-well plate) were used. The positive signals (duplicate spots) were measured using the Quantity One software (V.4.6.6, Bio-Rad, Hercules, California, USA) and the values (abundances of each cytokine) were normalized to the reference spots.

Osteoclastogenesis assay

RAW264.7 cells were seeded at 1.7×10^4 cells per well in 24-well plates. 24 hours later, 50 ng/mL recombinant mouse RANKL (Abcam) was added in growth culture medium in presence or absence of one RANKL inhibitor of interest (anti-RANKL (clone IK22/5, Bio X Cell, West Lebanon, New Hampshire, USA), RANK-Fc (Amgen, Thousand Oaks, California, USA), gallocatechin gallate (GCG, Sigma-Aldrich), isoliquiritigenin (Thermo Fisher Scientific), ampelopsin H (AOBIOUS, Gloucester, Massachusetts, USA) and L3-3B (Eurogentec)). For each compound, several concentrations were tested.

As previously described,[26][27] the cells were cultured for 6 days to induce RANKL-dependent osteoclast differentiation. After a washing step (phosphate-buffered saline (PBS)), the cells were collected and RNA extraction was performed using the NucleoSpin RNA isolation kit (Macherey-Nagel, Düren, Germany), according to the supplier's recommendations. In parallel with qPCR analyses, TRAP staining was performed as previously described[28] and the number of multinucleated (≥ 3 nuclei), violet-stained (TRAP-positive) cells in each culture condition was precisely determined by computerized counting (QuPath V.0.4.3 software for digital pathology image analysis).[29]

Syngeneic mouse models

All animal experiments were performed following recommendations established by the Federation of European Laboratory Animal Sciences Associations.

4T1 (5×10^5), 67NR (1×10^6) and E0771 (7.5×10^5) cells were orthotopically injected into the mammary fat pad of 8-week-old female BALB/c or C57BL/6J mice (Janvier Labs, Le Genest-Saint-Isle, France) (n=10 per condition). In some cases, similar experiments were performed with Nude RJ:ATHYM-Foxn1$^{nu/nu}$ mice (n=6 per condition). When tumor volume reached about 80–100 mm^3 (~10 days post tumor cell injection), mice were treated with RANKL inhibitors (anti-RANKL (clone IK22/5, 1 mg/kg per injection, Bio X Cell), RANK-Fc (1 mg/kg per injection, Amgen) or GCG (10 mg/kg per injection, Sigma-Aldrich)) alone or in combination with InVivoPlus monoclonal anti-mouse PD-1 antibody (clone 29F.1A12, 10 mg/kg per injection, Bio X Cell). Where indicated, combination treatments with 2.5 mg/kg doxorubicin (Selleckchem) or 10 mg/kg paclitaxel (Selleckchem) were also tested. For antibody-mediated Treg cell depletion, intraperitoneal injections of 200 µg (at day –1) and 100 µg (at days 4, 7 and 11) of InVivo monoclonal anti-mouse CD25 antibody (clone PC-61.5.3, Bio X cell) were performed. Tumor size was monitored with a digital caliper (Thermo Fisher Scientific) every 2–3 days and mice were euthanized when the mean tumor volume ((length × width^2) × π /6) of the control group exceeded 1200 mm^3 or at day 20. Half of the tumors were harvested, enzymatically dissociated using collagenase A (1 mg/mL, Sigma-Aldrich) and DNase (20 µg/mL, Sigma-Aldrich) before CD45$^+$ cell isolation/enrichment using CD45 microbeads (Miltenyi Biotec, Bergisch Gladbach, Germany) and flow cytometry analysis. Using this procedure, the proportion of dead immune cells (assessed using the Zombie Yellow fixable viability kit (BioLegend, San Diego, California, USA)) was always relatively low (comprised between 2.5 and 7% of total CD45$^+$ cells). The other retrieved tumors (as well as liver, lungs, spleen and kidneys) were fixed in 10% formalin, embedded in paraffin and sections were subjected to histological and/or immunohistochemical evaluations.

Flow cytometry (for in vivo experiments)

The proportions of 14 immune cell (sub)populations encountered within the mouse tumor microenvironment were determined using a FACSCanto II flow cytometer (GIGA in vitro imaging platform) and collected data were analyzed with FACSDiva software (V.6.1.2, BD Biosciences, San Jose, California, USA). Isolated CD45$^+$ cells were first incubated with anti-CD16/CD32 antibody (clone 2.4G2, BD Biosciences) for minimizing non-specific binding. The following immune cell (sub)populations were analyzed: B cells (CD45$^+$, CD19$^+$), CD4$^+$ T cells (CD45$^+$, CD3$^+$, CD4$^+$), CD8$^+$ T cells (CD45$^+$, CD3$^+$, CD8$^+$), CD4$^+$ Treg cells (CD45$^+$, CD3$^+$, CD4$^+$, CD25$^+$, FoxP3$^+$), CD8$^+$ Treg cells (CD45$^+$, CD3$^+$, CD8$^+$, CD25$^+$, FoxP3$^+$), DC (CD45$^+$, CD11b$^+$, I-A/I-E^{high}, F4/80$^-$), eosinophils (CD45$^+$, Ly6C$^-$, Siglec F$^+$), granulocytic myeloid-derived suppressor cells (MDSC) (CD45$^+$, CD11b$^+$, I-A/I-E^{int}, Ly6G$^+$, Ly6C$^-$), monocytic MDSC (CD45$^+$, CD11b$^+$, I-A/I-E^{int}, Ly6G$^-$, Ly6C^{high}), M1-like macrophages (CD45$^+$, CD11b$^+$, CD11c$^+$, F4/80$^+$, CD206$^-$), M2-like macrophages (CD45$^+$, CD11b$^+$, CD11c$^-$, F4/80$^+$, CD206$^+$), neutrophils (CD45$^+$, CD11b$^+$, I-A/I-E^{int}, Ly6G$^+$, Ly6C^{int}), natural killer (NK) cells (CD45$^+$, NKp46$^+$) and pDC (CD45$^+$, CD11b^{int}, CD11c$^+$, BST2$^+$, Siglec H$^+$). DC and pDC activation statuses were also determined by analyzing the membrane expression of CD80, CD86, I-A/I-E, ILT3 and CD80, CD86, I-A/I-E, ICOSL, respectively. All fluorochrome-conjugated anti-mouse antibodies used in this study are listed in online supplemental table 2. The precise gating strategy is shown in online supplemental figure 1.

Breast cancer metastasis model using intravenous tumor cell injection

Luciferase-expressing 4T1 cells (1×10^4) were intravenously injected in 8-week-old female BALB/c mice (Janvier Labs) (n=10 per condition). Mice were treated with anti-RANKL antibody (clone IK22/5, 1 mg/kg), RANK-Fc (1 mg/kg) or GCG (10 mg/kg) every 3 days for 21 days. At days 8, 11, 14, 17 and 21 post-cell injection in tail vein, in vivo imaging was performed using an IVIS Lumina III system (PerkinElmer, Waltham, Massachusetts, USA) and the average radiant efficiency (p/s/cm²/sr) was measured over the whole body. At the time of sacrifice, the main organs (lungs, liver, spleen, kidneys and brain) were collected and embedded in paraffin for H&E staining (in order to confirm the metastatic foci and to perform computerized analysis (QuPath V.0.4.3 software))).

Gene expression analysis (using public datasets)

The expression level of RANKL (*TNFSF11* gene) and its receptor RANK (*TNFRSF11A* gene) in 81 normal cell types from 31 published single-cell RNA sequencing datasets (30 different healthy human tissues and peripheral mononuclear cells (PBMCs) (online supplemental table 3)) was evaluated through the Human Protein Atlas interface (V.23.0, release date: June 19, 2023). Altogether, transcriptomics data from 689,601 human cells were

analyzed. In parallel, both RANKL and RANK messenger RNA (mRNA) levels in the most prevalent cancer subtypes (9,699 cancer samples divided into 28 subtypes) as well as in the four major breast cancer subclasses (luminal A (n=499), luminal B (n=197), HER2+ (n=78) and TNBC (n=171)) were assessed using The Cancer Genome Atlas (TCGA) public datasets (Pan-Cancer Atlas) through the cBioPortal interface.[30][31] At last, transcriptomic data from TNBC contained in the TCGA-breast cancer (BRCA) collection was retrieved and patients were split into groups based on *TNFRSF11A* and *TNFSF11* z-score normalized gene expression (top 25% vs bottom 25%). Differentially expressed genes were assessed between the two groups, including $\log_2$FC and p values for each gene. Gene set enrichment analysis (GSEA) and visualization were performed on significantly differentially expressed genes (p<0.05) using clusterProfiler (V.4.0)[32][33] and enrichplot (V.3.18) packages in R.

Boyden chamber migration assay

Chemotactic activity of RANKL (100 and 500 ng/mL) on both DC and pDC was assessed using a Boyden chamber assay (48-well Boyden microchamber; Neuro Probe, Gaithersburg, Maryland, USA), as described previously.[24] Non-conditioned medium supplemented with 0.2% bovine serum albumin (Sigma-Aldrich) and conditioned medium of human fibroblasts were used as negative and positive control, respectively. For each experimental condition, six wells were used. The cells having migrated were finally fixed, stained (Diff-Quick procedure) and two microscopic fields per well were randomly selected for quantification.

Immunohistochemistry and immunostaining assessment

After deparaffinization (in xylene) and rehydration (using decreased concentrations of ethanol) steps, the antigens were retrieved in citrate buffer (10 mM, pH 6) (Sigma-Aldrich). Endogenous peroxidases and non-specific binding sites were blocked using 4.5% H2O2 (Acros Organics, Geel, Belgium) and serum-free Protein Block reagent (Dako/Agilent Technologies, Glostrup, Denmark), respectively. Anti-RANKL (1/100, ab216484; Abcam), anti-RANK (1/200, LS-B2077; LSBio, Seattle, Washington, USA), anti-CD45 (1/1000, ab10558; Abcam), anti-CD3 (ready to use, clone 2GV6; Ventana Medical Systems, Tucson, Arizona, USA), anti-CD4 (ready to use, clone SP35; Ventana Medical Systems), anti-CD8 (ready to use, clone SP57; Ventana Medical Systems), anti-mouse Foxp3 (1/200, clone D6O8R; Cell Signaling Technology, Danvers, Massachusetts, USA), anti-human Foxp3 (1/100, clone 236A/E7; Thermo Fisher Scientific), anti-CD68 (ready to use, clone KP-1; Ventana Medical Systems) and anti-CD206 (1/600, clone E6TSJ; Cell Signaling Technology) antibodies were used for the primary reaction. After a washing step (PBS), mouse or rabbit EnVision detection system (Dako) was used for the secondary reaction. Finally, positive cells were visualized

using SignalStain DAB Substrate Kit (Cell Signaling Technology).

As previously described,[34][35] both the intensity (0: negative; 1: low; 2: moderate; 3: strong) and the extent (0: <5%; 1: 6–33%; 2: 34–66%; 3: >67%) of anti-RANKL and anti-RANK immunostainings displayed by tumor cells were evaluated by independent and experienced pathologists, according to an arbitrary scale. The results obtained with the two scales were multiplied in order to obtain a global score for each case comprised between 0 and 9. Regarding the total intratumoral immune cells (CD45+) and various specific subpopulations (CD3+, CD4+, CD8+, CD68+, CD206+ and Foxp3+), the number of positive cells per mm^2 was determined by computerized counting (QuPath V.0.4.3 or V.0.5.1 software) and verified by manual counting.

Quantitative reverse transcription PCR

The reverse transcription step was performed as previously described (one µg total RNA/reaction).[36] qPCR experiments (QuantStudio 3, Applied Biosystems, Foster City, California, USA) were then run using the FastStart Universal SYBR Green Master mix (Roche) and the following primer sequences: CTSK forward: 5'-GTT GTA TGT ATA ACG CCA CGG C-3'; CTSK reverse: 5'-CTT TCT CGT TCC CCA CAG GA-3'; TRAP forward: 5'-GCT ACT TGC GGT TTC ACT ATG GA-3'; TRAP reverse: 5'-TGG TCA TTT CTT TGG GGC TTA TCT-3'; Foxp3 forward: 5'-GCA CCT TCC CAA ATC CCA GT-3'; Foxp3 reverse: 5'-GGC CAC TTG CAG ACA CCA T-3'; CD25 forward: 5'-GAG ACT TCC TGC CTC GTC ACA A-3'; CD25 reverse: 5'-GAT CAG CAG GAA AAC ACA GCC G-3'; CD69 forward: 5'-GCT GGA CTT CAG CCC AAA ATG C-3'; CD69 reverse: 5'-AGT CCA ACC CAG TGT TCC TCT C-3'; Helios forward: 5'-ACA CTC TGG AGA GAA GCC GTT C-3'; Helios reverse: 5'-CCA GTG AAC TGC GCT GCT TGT A-3'; Neuropilin-1 forward: 5'-AAC AAC GGC TCG GAC TGG AAG A-3'; Neuropilin-1 reverse: 5'-GGT AGA TCC TGA TGA ATC GCG TG-3'; 18S forward: 5'-ACC CGT TGA ACC CCA TTC GTG A-3'; 18S reverse: 5'-GCC TCA CTA AAC CAT CCA ATC GG-3'. 18S was used as an internal control and collected results were analyzed using the $2^{-(\Delta\Delta Ct)}$ method. Each experiment was performed in duplicate.

Western blot

Cells were lysed in 1% sodium dodecyl sulfate (SDS) buffer containing protease and phosphatase inhibitors (Roche). Protein quantification was performed using the BCA protein assay kit (Pierce, Rockford, Illinois, USA). 10 µg of proteins were separated on 6% or 10% SDS-polyacrylamide gel electrophoresis and transferred to polyvinylidene fluoride membranes (Roche). After a blocking step in tris-buffered saline(TBS)-Tween 0.1% containing 5% bovine serum albumin, the membranes were incubated overnight at 4°C with the following primary antibodies: anti-mTOR (1/1000, clone 7C10; Cell Signaling Technology), anti-phospho mTOR (1/1000,

clone D9C2; Cell Signaling Technology), anti-p70 S6 kinase (1/1000, #9202; Cell Signaling Technology), anti-phospho p70 S6 kinase (1/1000, clone 108D2; Cell Signaling Technology), anti-S6 ribosomal protein (1/1000, clone 5G10; Cell Signaling Technology), anti-phospho S6 ribosomal protein (1/1000, #2211; Cell Signaling Technology), anti-Hamartin/TSC1 (1/1000, #4906; Cell Signaling Technology), anti-Tuberin/TSC2 (1/1000, clone D93F12; Cell Signaling Technology), anti-phospho Tuberin/TSC2 (1/1000, clone 5B12; Cell Signaling Technology), anti-Akt (1/1000, #9272; Cell Signaling Technology), anti-phospho Akt (1/1000, clone D9E; Cell Signaling Technology), anti-p85 PI3K (1/1000, #4292; Cell Signaling Technology), anti-phospho p85/ p55 PI3K (1/1000, #4228; Cell Signaling Technology), anti-TRAF6 (1/1000, clone D21G3; Cell Signaling Technology) and anti-β-actin (1/2000, clone AC-15; Sigma-Aldrich). The membranes were washed with TBS-Tween 0.1% and then incubated with an anti-rabbit (1/2000, #7074; Cell Signaling Technology) or anti-mouse (1/2000, #7076; Cell Signaling Technology) antibody for 1 hour at room temperature. The protein bands were finally visualized using an ImageQuant 800 biomolecular imager (Cytiva, Amersham, UK) and quantified by densitometric analysis (ImageJ software, National Institute of Health, Bethesda, Maryland, USA).

ELISA

Mouse and human TNBC cells (1×10^6 per well in a 6-well plate) were cultured in appropriate growth medium during 48 hours. Cell culture supernatants were then collected and RANKL release was quantified using the RANKL/TNFSF11 ELISA Kit (ab100749, Abcam) according to the manufacturer's protocol. At the end of the experiment, the number of alive cells in each well was also determined precisely in order to normalize collected RANKL concentrations (pg/mL per 10^6 cells).

Cell proliferation

Cells were seeded in 24-well plates in order to reach~10% confluence. Cell proliferation under indicated culture conditions was then monitored for 5 days using the Incucyte Live-Cell Analysis System (Sartorius, Goettingen, Germany) (GIGA in vitro imaging platform, University of Liege). Pictures (four fields per well) were taken every 6 hours and accumulated information was finally analyzed using the Incucyte software.

Apoptosis

Following an incubation for 48 hours with each individual RANKL inhibitor, the percentages of early and late apoptotic cancer cells were determined by flow cytometry (FACSCalibur, BD Biosciences) using annexin V-FITC and propidium iodide staining (Thermo Fisher Scientific) and summed. The gating strategy is shown in online supplemental figure 1.

Metabolic extracellular flux analysis

Mouse TNBC cells (10,000 per well) were first seeded in a specific Seahorse XFp mini-plate (Agilent, Santa Clara, California, USA) and each individual RANKL inhibitor was then added to the medium. After 16 hours, the medium was changed and the cells were incubated with unbuffered serum-free DMEM (pH 7.4) containing 1 mM pyruvate, 2 mM glutamine and 10 mM glucose for 1 hour. To measure the oxygen consumption rate, cells were successively stressed with 1 μM oligomycin, 1 μM carbonyl cyanide-p-trifluoromethoxyphenylhydrazone and 0.5 μM rotenone/antimycin A. For each condition, collected data were normalized to the cell number.

Statistical analysis

Statistical analysis was performed using GraphPad Prism V.8.3 software (San Diego, California, USA). (Welch-corrected) unpaired student's t-test and one-way analysis of variance (ANOVA) followed by Dunnett's or Bonferroni multiple comparison post hoc test were used to assess the statistical significance between two and more groups/conditions, respectively. Where indicated, one sample t-test was used to determine whether the mean from an individual group was different from a specific value. In the case of discrete variables (immunohistochemical scores, aneuploidy,[37] Buffa hypoxia score,[38] age at diagnosis, number of metastatic foci), a Mann-Whitney or Kruskal-Wallis ANOVA test followed by Dunn post hoc test was performed according to the number of groups. The comparison of tumor characteristics (tumor size, nodal status, tumor type, *TP53* mutation, treatment modality) between independent groups was performed using a χ^2 test. The Kaplan-Meier method was used to estimate both the progression-free and overall survivals based on TCGA-BRCA data. Survival curves were compared using a Log-rank (Mantel-Cox) test. The correlation between RANKL expression and the density of various immune cells within the tumor microenvironment was assessed using Spearman's rank correlation test. *p<0.05, **p<0.01, ***p<0.001 and ****p<0.0001.

RESULTS
RANKL is highly expressed by hormone receptor/HER2-negative breast cancer cells and significantly associated with enriched immune regulation/differentiation gene signatures

By using public single-cell RNA sequencing datasets (from 30 healthy human tissues and PBMCs), a detailed overview of the RANKL/RANK ligand–receptor pair expression level in normal cells was first generated (figure 1A,B). To do so, transcriptomic data from 689,601 cells (subclassified into 81 different cell types) were analyzed. Although higher mRNA levels are noticed in glandular epithelial cells (especially those lining the gastrointestinal (GI) tract), RANK expression seems to be relatively ubiquitous, as attested by transcripts detected in most normal cell types (69/81, 85.2%). As for RANKL, its expression is more restricted (39/81, 48.1%) and peaks in breast
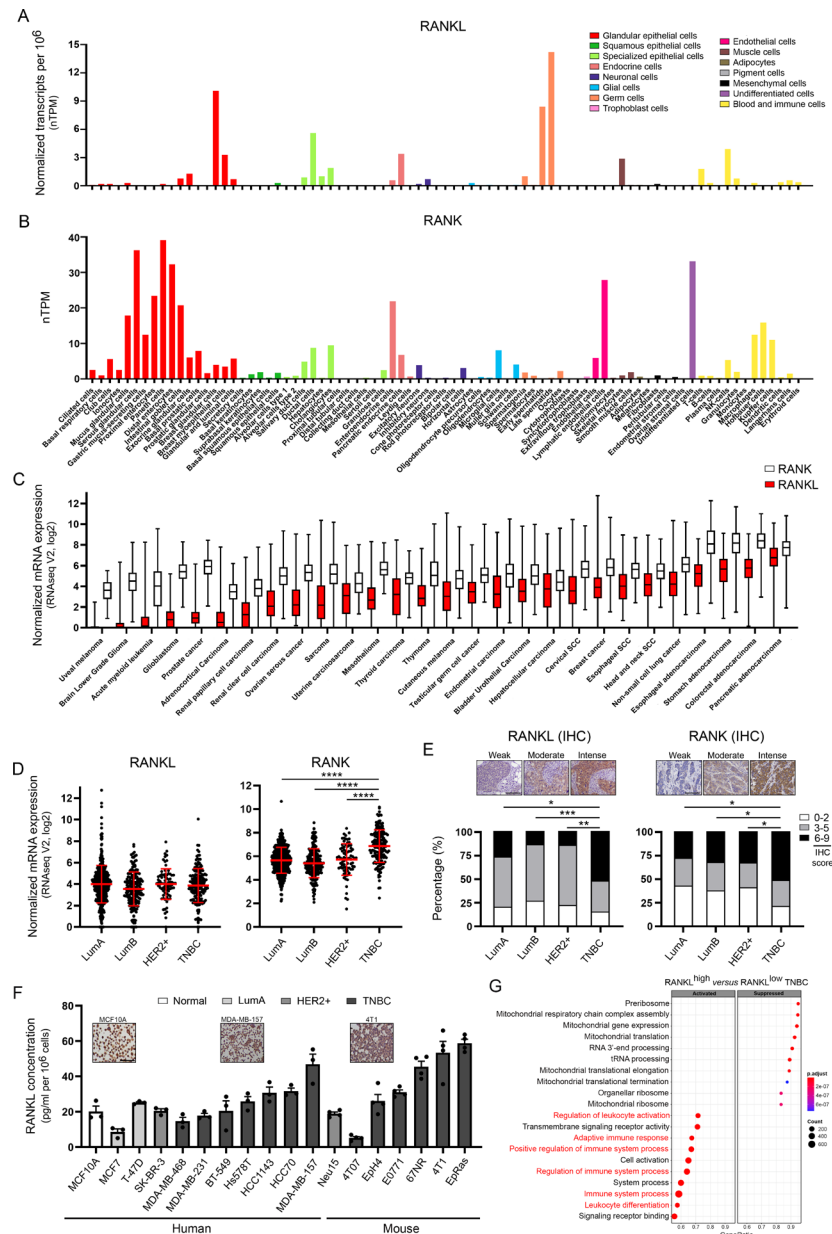
Figure 1 An elevated expression of RANKL is detected in neoplastic mammary glands (especially those negative for both the hormone receptors and HER2) and associated with a significant rise in immune-related transcripts. The mRNA expression level of RANKL (A) and RANK (B) was assessed in 81 normal cell types using 31 different single-cell RNA sequencing datasets from healthy human tissues (available through the Human Protein Atlas interface). (C) By reviewing datasets (n=28) being part of the TCGA Research Network and comprizing at least 50 individual samples, the expression of *TNFSF11* (RANKL, in red) and *TNFRSF11A* (RANK, in white) genes was evaluated in the most prevalent cancer subtypes. (D) Using specifically TCGA-BRCA data, both RANKL and RANK expression levels were investigated in breast neoplasms. All tumors were classified according to their molecular subtypes (LumA, n=499; LumB, n=197; HER2+, n=78; TNBC, n=171). (E) Semiquantitative evaluation of RANKL and RANK expression (intensity and extent of the immunostainings) displayed by human breast cancers (LumA, n=38; LumB, n=40; HER2+, n=49; TNBC, n=56). Representative examples of immunolabeled human breast cancer specimens are shown. (F) RANKL concentrations detected by ELISA in human and mouse cell culture media. High protein levels were especially observed in supernatants derived from TNBC cells. The means±SEM (plus each individual data point) for three (human cells) or four (murine cells) independent experiments are represented. Representative pictures of normal (MCF10A) and malignant cell lines (human: MDA-MB-157; mouse: 4T1) stained for RANKL are also shown. (G) Dot plots illustrating the significant Top 10 positively and negatively enriched GO biological processes associated with high RANKL expression in the context of TNBC (gene set enrichment analysis). The highlighting of several immune-associated gene signatures (in red) should be noticed. The scale bar represents 100 µm. Asterisks indicate statistically significant differences (*p<0.05; **p<0.01; ***p<0.001; ****p<0.0001). P values were determined using one-way ANOVA followed by Bonferroni post-test (D) and Kruskal-Wallis ANOVA test followed by Dunn post hoc test (E). ANOVA, analysis of variance; GO, Gene Ontology; HER2+, human epidermal growth factor receptor 2+; IHC, immunohistochemistry; mRNA, messenger RNA; NK, natural killer; RANKL, receptor activator of nuclear factor κB ligand; SCC, squamous cell carcinoma; TCGA, The Cancer Genome Atlas; TNBC, triple-negative breast cancer; tRNA, transfer RNA.

glandular cells, pancreatic ductal cells and early/late spermatids. In parallel, the expression levels of *TNFSF11* (RANKL) and *TNFRSF11A* (RANK) genes were investigated in various (the most prevalent) tumor subtypes (n=28) using individual datasets being part of the TCGA Research Network. While RANK mRNA expression is relatively stable across cancers, its ligand displayed a more important heterogeneity and is predominantly detected in breast and lung neoplasms as well as in tumors diagnosed in the upper/lower GI tract (figure 1C). Based on these transcriptomic data (and the availability of several immunocompetent in vivo models allowing us to study novel anticancer drugs with possible immunotherapeutic properties), we decided to focus our attention on breast cancer. Although the statistical significance was not reached for RANKL at the mRNA level, importantly, the RANKL/RANK axis has been shown to be overexpressed in triple-negative neoplasms compared with their counterparts expressing hormone (estrogen and progesterone) receptors and/or HER2. The results collected at the mRNA and protein level are shown in figure 1D,E, respectively. Remarkably, the prognostic value of RANKL expression was also highlighted in the specific context of TNBC. Indeed, patients from the TCGA-BRCA collection with RANKL^high-expressing TNBC were associated with a favorable outcome (online supplemental figure 2A,B). Importantly, this evidence of improvement in both progression-free and overall survivals cannot be explained by differences in age at diagnosis, tumor size, nodal/metastatic status, tumor type, hypoxia score, *TP53* mutation status, aneuploidy score or treatment modality (online supplemental figure 2C). Confirming both transcriptomic and ex vivo/immunohistochemical findings, most mouse/human cell lines displayed intense immunoreactivity for RANKL (especially those derived from TNBC) and high protein concentrations were measured by ELISA in cell culture supernatants (figure 1F). To determine both activated and suppressed biological processes associated with high RANKL expression, TNBC samples from the TCGA-BRCA dataset were clustered on the basis of *TNFSF11* mRNA level (top 25% vs bottom 25%) and GSEA was performed on differentially expressed genes using standard GO categorizations. As shown in figure 1G and listed in online supplemental table 4, the significant Top 10 negatively and positively enriched GO terms in RANKL^high-expressing tumors were mainly related to mitochondrial functions and immune regulation/differentiation (6 out of 10), respectively. Of note, a similar in silico analysis was done with the receptor RANK and, strikingly, the significant transcriptomic changes were much fewer, with an absence of enrichment of immune-associated genes. To further confirm the link between RANKL and immune system regulation, the correlation between RANKL expression and the density of various immune cells within the tumor microenvironment was assessed in primary TNBC and in the lungs (in the case of metastatic dissemination). Interestingly, while the overall number of immune cells (CD45+), macrophages (CD68+)

and T cells (CD3+, CD4+, CD8+) remained relatively unaffected (an increasing trend was observed with higher RANKL positivity, but statistical significance was not reached), RANKL expression was significantly correlated with the densities of both Foxp3+ (Treg) and CD206+ (M2-like macrophages) cells in primary tumors (online supplemental figure 3).

Both direct and indirect RANKL inhibitors efficiently neutralize soluble RANKL without affecting cancer cell proliferation/viability

In the last decade, several direct (anti-RANKL antibody, RANK-Fc (chimeric protein formed by fusing the extracellular domain of RANK with the constant region of human immunoglobulin G1), L3-3B (13-amino-acid peptide mimicking Loop3 of RANK), ampelopsin H (natural compound isolated from *Parthenocissus tricuspidata*, commonly called Virginia Creeper) or indirect (GCG (major active compound in green tea), isoliquiritigenin (chalcone derived from the licorice)) RANKL inhibitors (acting following different modes of inhibition) have been reported in the literature (figure 2A).[39–43] Of note, we chose not to include the decoy receptor OPG in this study due to concerns raised in previous clinical trials about the potential for a neutralizing immune response against endogenous OPG.[44] Additionally, OPG can bind to multiple ligands beyond RANKL, notably the tumor necrosis factor-related apoptosis-inducing ligand,[45] which plays a crucial role in the antitumor cytotoxicity mediated by various immune populations (eg, macrophages, neutrophils, DC, pDC, NK cells)[46 47] and could, therefore, introduce significant bias in the assessment of the immunotherapeutic efficacy of RANKL blockade. In order to test the efficacy of each individual preselected RANKL inhibitor (and, ultimately, to determine the effective concentrations that inhibit RANKL activity by>80%), murine RAW 264.7 cells were stimulated with recombinant RANKL alone or in the presence of graded concentrations of each inhibitor. RANKL-dependent osteoclastogenesis was then determined by quantifying the mRNA level of two osteoclast-specific enzymes (TRAP and CTSK) as well as by TRAP staining (figure 2B–D). Remarkably, both TRAP and CTSK expressions were maintained at their basal level following the addition of anti-RANKL antibody or RANK-Fc (0.5–1 µg/mL), indicating the complete neutralization of RANKL activity. Regarding GCG, an over 80% efficiency to block soluble RANKL was shown at concentrations of 10 µg/mL or greater. A partial (up to 60%) inhibition of RANKL-induced TRAP/CTSK expression was observed with isoliquiritigenin. As for L3-3B and ampelopsin H, no efficient neutralizing RANKL activity was reported. These results collected by qPCR analysis were clearly confirmed after TRAP staining. Indeed, the number of multinucleated, violet-stained (TRAP-positive) cells was reduced by>90% following the addition of anti-RANKL antibody, RANK-Fc and GCG in RANKL-stimulated RAW264.7 culture medium. The limited inhibition of RANKL-dependent
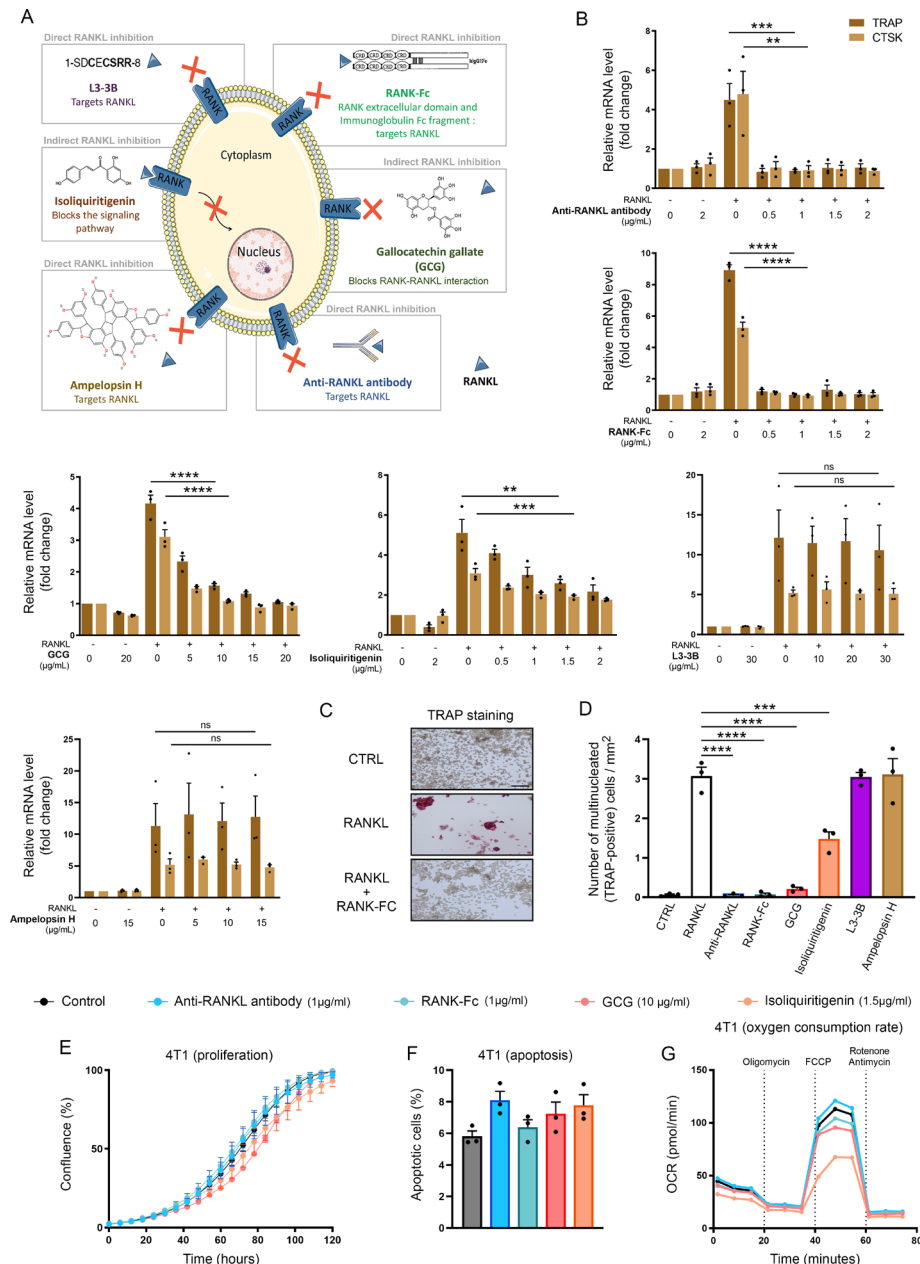
Figure 2 Anti-RANKL antibody, RANK-Fc and Gallocatechin gallate (GCG) exert efficient neutralizing effect on extracellular RANKL without altering cancer cell proliferation, apoptosis and metabolism. (A) Schematic representation of RANKL inhibitors tested in the present study as well as their respective mode of inhibition. (B) Murine RAW 264.7 cells were stimulated with recombinant RANKL alone or in the presence of graded concentrations of each RANKL inhibitor for 6 days. TRAP and CTSK mRNA levels were then determined by RT-qPCR in order to assess the efficiency of each individual inhibitor in blocking RANKL-dependent osteoclastogenesis. Note the significant downregulation of these two osteoclast markers when anti-RANKL antibody, RANK-Fc, GCG and isoliquiritigenin were added in the cell culture media. Results represent the means±SEM of three independent experiments performed in duplicate. (C) In parallel, the neutralizing activity of each RANKL inhibitor was also determined by TRAP staining. Representative pictures of untreated or treated RAW 264.7 cells are shown. (D) Number of multinucleated (≥ 3 nuclei), violet stained (TRAP-positive) cells per mm^2 in each culture condition (anti-RANKL antibody (1 µg/mL), RANK-Fc (1 µg/mL), GCG (10 µg/mL), isoliquiritigenin (1.5 µg/mL), L3-3B (10 µg/mL), Ampelopsin H (10 µg/mL)). Results represent the means±SEM of three independent experiments. (E) Proliferation, (F) apoptosis and (G) oxygen consumption rate (OCR) of 4T1 cells in the absence or presence of anti-RANKL antibody (1 µg/mL), RANK-Fc (1 µg/mL), isoliquiritigenin (1.5 µg/mL) and GCG (10 µg/mL) were determined using Incucyte live cell analyzing system, annexin V-propidium iodide staining assay and Seahorse extracellular flux analyzer, respectively. The decrease of OCR when cancer cells were treated with isoliquiritigenin should be noticed. Results represent the means±SEM (each individual data point is shown). The scale bar represents 100 µm. Asterisks indicate statistically significant differences (**p<0.01; ***p<0.001; ****p<0.0001). P values were determined using one-way ANOVA followed by Dunnett's multiple comparison post hoc test (B, D, E, F). ANOVA, analysis of variance; FCCP, carbonyl cyanide-p-trifluoromethoxyphenylhydrazone;mRNA, messenger RNA; ns, not significant; RANKL, receptor activator of nuclear factor κB ligand; RT-qPCR, quantitative reverse transcription PCR.
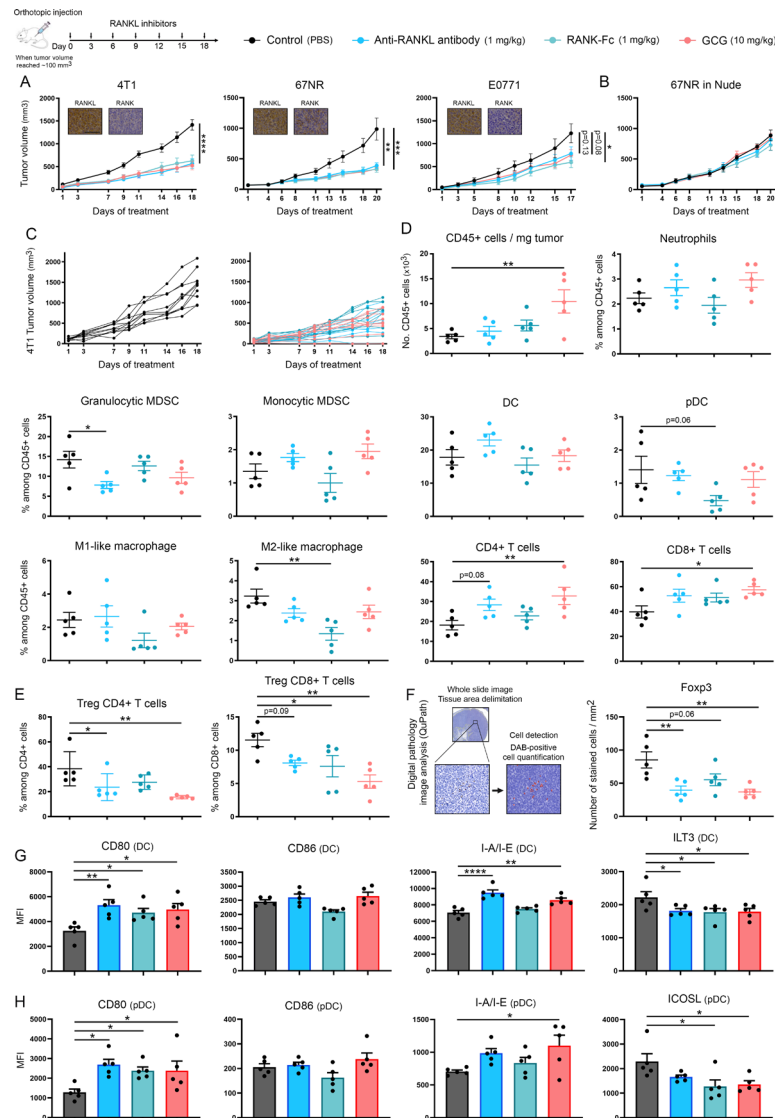
osteoclast differentiation in the presence of isoliquiritigenin as well as the lack of effect of both L3-3B and ampelopsin H were also verified. The effect of efficient RANKL inhibitors on cancer cell proliferation, apoptosis and metabolism was then precisely determined using the Incucyte live cell analyzing system, annexin V-propidium iodide staining assay and Seahorse flux analyzer, respectively (figure 2E–G and online supplemental figure 4). Whereas anti-RANKL antibody (1 µg/mL), RANK-Fc (1 µg/mL) and GCG (10 µg/mL) did not affect these three cellular parameters, the mitochondrial respiration (and, more precisely, the maximal respiratory capacity of cells) was strongly reduced in the presence of isoliquiritigenin, suggesting that this indirect RANKL inhibitor targeting downstream signaling cascades alters cell energetic metabolism (glycolysis). Based on these latter results as well as its partial efficiency to block RANKL activity, isoliquiritigenin was not kept for our in vivo experiments.

RANKL blockade inhibits tumor growth in various syngeneic mouse TNBC models through activating adaptive immune responses

Next, we sought to determine the antitumor effects of RANKL blockade. To do so (and to mimic human disease closely), murine TNBC cells (4T1, 67NR or E0771) were orthotopically injected (into the mammary fat pad) and, when solid tumors reached approximately 80–100 mm^3, mice were treated with RANKL inhibitors at 3-day intervals for up to 20 days. As commonly practiced, the concentration used in vivo for each inhibitor (anti-RANKL antibody (1 mg/kg), RANK-Fc (1 mg/kg), GCG (10 mg/kg)) was extrapolated from our in vitro findings (figure 2) by considering that mol or g/L~mol or g/kg for compounds diluted in liquid solutions (PBS). All three cancer models displayed intense RANKL immunoreactivity whereas the expression of its receptor by tumor cells was weak (4T1 and E0771) or moderate (67NR). As shown in figure 3A, a striking decrease in tumor growth was observed in both 4T1 and 67NR models using all three RANKL inhibitors. A complete tumor elimination (below palpable detection) was even observed in 10% (3 out of 30) treated mice bearing 4T1 tumors (figure 3C). This reduced tumor growth following RANKL blockade was also detected in the E0771 model, but to a lesser extent. Overall, when data (at the endpoints) were pooled, treated mice transplanted with 4T1, 67NR and E0771 cells displayed mean tumor growth inhibitions of 59.5%, 65.2%, and 41.9%, respectively. Notably, not only did RANKL inhibitors greatly diminish primary tumor development, but also the metastatic dissemination of TNBC cells was significantly impaired. Indeed, as shown in online supplemental figure 5, both the number and average size of 4T1 lung metastatic foci were significantly reduced following RANKL blockade. 67NR and E0771 cells did not colonize distant tissues. To further confirm these results, another breast cancer metastasis model, in which luciferase-expressing tumor cells are injected intravenously (in tail vein), was performed. Whereas no metastatic nodule was detected in the liver, spleen, kidneys and brain, both the bioluminescence results and H&E staining images indisputably confirmed the presence of metastatic foci in the lungs and, importantly, their significant reduction in mice treated with RANKL inhibitors (online supplemental figure 5G–K). Finally, it is important to notice that no reduction in (primary) tumor size was observed in immunocompromised Nude mice, clearly indicating that the antitumor properties of RANKL inhibitors are dependent on the adaptive immune responses (figure 3B).

After 20 days of treatment (or when the average tumor volume of the control group reached 1200 mm^3), tumors were harvested and the number of CD45$^+$ cells per milligram of tumor as well as the percentage of 12 individual immune cell populations (neutrophils, granulocytic and monocytic MDSC, DC, pDC, M1-like and M2-like macrophages, CD4$^+$ and CD8$^+$ T cells, NK cells, eosinophils and B cells) among total CD45$^+$ cells were analyzed by flow cytometry in both control and treated groups. Additionally, the proportions of Treg cells among total CD4$^+$/CD8$^+$ cells and the activation status of antigen-presenting cells (DC and pDC) were also determined. Despite minor variations (related to in vivo experiments, models and/or drugs used), two main observations were reproducibly made in the groups treated with RANKL inhibitors compared with controls: (1) without affecting the global number of CD4$^+$/CD8$^+$ lymphocytes, a drastic loss of Treg cells (by up to 70%) was observed and (2) an increased activation of both DC and pDC was detected (as demonstrated in particular by the constant upregulation of CD80 associated with the reduced expression of ILT3 (DC) or ICOSL (pDC)) (figure 3D–H, online supplemental figures 6 and 7). Determined by immunohistochemistry and subsequent computerized counting, a reduced Foxp3$^+$ cell infiltration within the tumor microenvironment following RANKL blockade further confirmed the flow cytometry results (figure 3F). Concurrently, the percentage of M2-like macrophages also tended to decrease in the case of RANKL inhibition, but the statistical significance was not reached in most conditions. The other immune cells did not appear to be affected by the presence (or absence) of RANKL. To assess whether the strong diminution of intratumoral Treg cells actively participates in the beneficial (antitumor) effect of RANKL inhibitors, antibody-mediated depletion experiments were performed. As shown in figure 4, anti-CD25 antibody treatment induced a significant loss of tumor-infiltrating Treg cells and, more importantly, this depletion reduced RANKL blockade-dependent tumor growth inhibition by more than 50%. Because, whatever the model used, their proportions never exceeded 1% of the total tumor-infiltrating immune cells (data not shown), we decided to no longer evaluate eosinophils, NK cells and B cells in the following parts of this study.
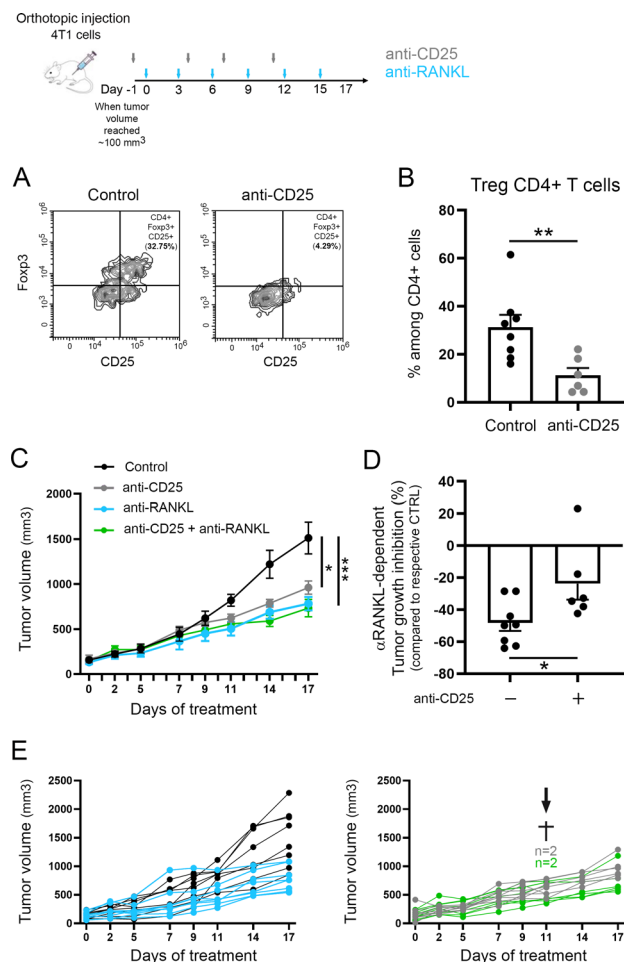
Figure 3 RANKL blockade inhibits the growth of pre-established breast tumors in immunocompetent mice through activating anticancer immunity. (A) Mouse TNBC cells (4T1, 67NR and E0771) were orthotopically injected into the mammary fat pad of immunocompetent BALB/c (4T1 and 67NR) or C57BL/6J (E0771) mice. Tumor-bearing mice were treated with RANKL inhibitors (anti-RANKL antibody (1 mg/kg), RANK-Fc (1 mg/kg) and GCG (10 mg/kg)) or PBS (control) at 3-day intervals. The mean tumor volumes±SEM are represented. RANKL/RANK immunoreactivities exhibited by TNBC tumors are also shown. While all three cancer models highly expressed RANKL, the anti-RANK immunoreactivity displayed by 4T1/E0771 and 67NR was weak and moderate, respectively. (B) RANKL inhibitors were also tested in Nude RJ:ATHYM-Foxn1$^{nu/nu}$ mice. The lack of anticancer effect in these immunocompromised mice should be noticed. (C) Single growth curves of 4T1 tumors treated or not with a RANKL inhibitor (PBS (n=10), anti-RANKL antibody (n=9), RANK-Fc (n=9), GCG (n=9)). (D) On day 18, 4T1 tumors were retrieved and enzymatically dissociated before flow cytometry analysis. Scatter dot plots showing the total number of (CD45$^+$) immune cells per milligram of tumor as well as the percentage of each individual immune cell population (neutrophils, granulocytic and monocytic MDSC, DC, pDC, M1-like and M2-like macrophages, CD4$^+$ and CD8$^+$ T cells) among CD45$^+$ cells in the different treated groups. The tumor-infiltrating immune cells were analyzed in 5 mice per condition. (E) Scatter dot plots illustrating the percentage of intratumoral CD4$^+$ and CD8$^+$ Treg (Foxp3$^+$, CD25$^+$) cells among total CD4$^+$ and CD8$^+$ subpopulations in the different groups of treated mice implanted with 4T1. Note the reduced proportions of Treg cells among total CD4$^+$/CD8$^+$ cells in the case of RANKL blockade. (F) The density of tumor-infiltrating Treg cells was determined by computerized counting (using QuPath software). The number of Foxp3$^+$ cells was reported to tumor area (mm^2). The activation status of both tumor-infiltrating DC (G) and pDC (H) in mice treated or not with a RANKL inhibitor was also determined by analyzing the expression of several surface markers (CD80, CD86, I-A/I-E, ILT3 (DC) and ICOSL (pDC)) by flow cytometry. Data represent the mean fluorescent intensity (MFI)±SEM of 5 independent analyzes in each group (each individual data point is shown). The scale bar represents 100 µm. Asterisks indicate statistically significant differences (*p<0.05; **p<0.01; ***p<0.001; ****p<0.0001). P values were determined using one-way ANOVA followed by Dunnett's multiple comparison post hoc test (A, D, E, G, H) or (Welch-corrected) unpaired t-test (F). ANOVA, analysis of variance; DAB, 3,3'-diaminobenzidine;DC, dendritic cell; GCG, gallocatechin gallate; MDSC, myeloid-derived suppressor cell; PBS, phosphate-buffered saline; pDC, plasmacytoid dendritic cell; RANKL, receptor activator of nuclear factor κB ligand; TNBC, triple-negative breast cancer; Treg, T regulatory.

Figure 4 In vivo depletion of Treg cells significantly alters RANKL blockade-dependent tumor growth inhibition. (A) Representative flow cytometry analysis showing the efficacy of anti-CD25-mediated cellular depletion. (B) Scatter dot plots illustrating the percentage of tumor-infiltrating Treg (CD25$^+$/Foxp3$^+$) CD4$^+$ among total CD4$^+$ populations in the control and anti-CD25-treated groups of mice implanted with 4T1 cells. An efficient and durable depletion was reported in the tumor microenvironment at the time of sacrifice. (C) 4T1 cells were orthotopically injected into the mammary fat pad of immunocompetent BALB/c mice. Control and Treg cell-depleted mice were treated at 3-day intervals with PBS (control) or anti-RANKL antibody (1 mg/kg). The mean tumor volumes±SEM are represented (n=8 per condition). (D) At day 17, the tumor growth inhibition induced by RANKL blockade in presence or absence of Treg cells was determined. To do so, the volume of each harvested anti-RANKL-treated tumor was compared with the average tumor volume obtained in the control or anti-CD25-treated group. The means±SEM (plus each individual data point) are represented. (E) Single growth curves of 4T1 tumors treated with anti-RANKL, anti-CD25 or both. Of note, a 25% mortality was observed in tumor-bearing mice on the fourth injection of anti-CD25 antibody. Asterisks indicate statistically significant differences (*p<0.05; **p<0.01; ***p<0.001). P values were determined using unpaired t-test (B, D) or one-way ANOVA followed by Bonferroni post-test (C). ANOVA, analysis of variance; PBS, phosphate-buffered saline; RANKL, receptor activator of nuclear factor κB ligand; Treg, T regulatory.

Neoadjuvant chemotherapy (but not PD-1 checkpoint inhibition) enhances the anticancer efficacy of RANKL blockade in immunocompetent mice

To determine whether RANKL blockade may boost anti-PD1-mediated enhancement of immune responses, combination treatments were performed. Importantly, data from our group and others previously reported high percentages of PD1$^+$ cells among both CD4$^+$ and CD8$^+$ lymphocytes as well as a partial antitumor efficacy of anti-PD-1 inhibition in mouse TNBC models.[25 48 49] As shown in figure 5A,B, anti-PD-1 antibody and RANKL inhibitors (RANK-Fc and GCG) displayed close therapeutic effectiveness and the combination therapy showed no benefit compared with anti-PD-1 or each RANKL inhibitor used in monotherapy. Of note, unlike RANKL inhibitors which have always been well tolerated (no apparent macro/microscopic signs of toxicity), 50% mortality in tumor-bearing mice was observed in the groups receiving anti-PD-1 antibody (rapid and fatal hypersensitivity reaction manifested after the third administration of anti-PD-1 inhibitor, as recently described in the literature[25 50] (figure 5C).

Given that chemoimmunotherapy represents a new trend in the treatment of various cancers (for a review, see the study by Sordo-Bahamonde *et al*[51]), we then decided to evaluate the potential benefit of the combination of neoadjuvant chemotherapy and RANKL blockade. As shown in figure 6 (67NR model), doxorubicin or paclitaxel-based chemotherapy plus RANKL inhibition was characterized by increased percentages of tumor-infiltrating CD4$^+$ and CD8$^+$ T cells (while maintaining both RANKL blockade-dependent decreased percentage of Treg cells and increased DC/pDC activation) and resulted in significantly greater tumor growth inhibition (by approximately 30%) than did either treatment alone. Of note, doxorubicin and paclitaxel potentiated the anticancer effects of RANKL blockade in a similar manner. While maintaining the reduction in metastatic dissemination observed with each individual RANKL inhibitor (online supplemental figure 8), a comparable increase in the number of both CD4$^+$ and CD8$^+$ T lymphocytes within the tumor microenvironment as well as a greater anticancer efficacy on primary (pre-existing) tumors was also observed in another TNBC model (4T1) treated with combination therapy (online supplemental figure 9).

RANKL acts as a tolerogenic signal on antigen-presenting cells (DC/pDC) through inhibiting mTOR signaling pathway

To further confirm our in vivo data and, overall, to validate the immunosuppressive activity of RANKL during cancer development/progression, several in vitro assays using human primary DC (figure 7) or pDC (online supplemental figure 10) were performed. Without exhibiting a chemotactic activity (figure 7A and online supplemental figure 9A), RANKL significantly altered the phenotype of both DC and pDC (figure 7B,C and online supplemental figure 10B,C) and induced a defect in the functional activity of these antigen-presenting
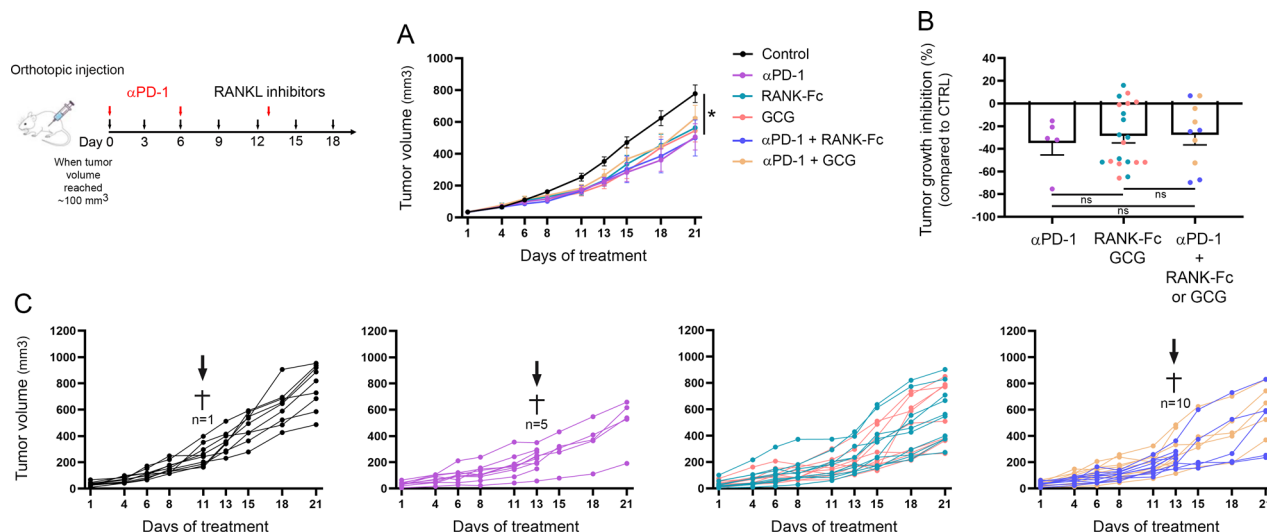
Figure 5 No synergistic antitumor effect is detected in the case of combined RANKL and PD-1 blockade. (A) Mouse TNBC 67NR cells were orthotopically injected into the mammary fat pad of immunocompetent BALB/c mice. Anti-PD-1 antibody was tested alone (10 mg/kg per i.p. injection at days 0, 6 and 13) and in combination with RANKL inhibitors (RANK-Fc (1 mg/kg) and GCG (10 mg/kg), treatment at 3-day intervals). In order to precisely determine the potential additive or synergistic effect of combination therapies, each individual RANKL inhibitor was also used in monotherapy. The mean tumor volumes±SEM are represented. (B) Following mouse euthanasia, the final volume of each resected tumor was determined, allowing the assessment of tumor growth inhibition induced by anti-PD-1 antibody, RANK-Fc or GCG alone as well as by the combination regimens. Each individual tumor volume was compared with the average tumor volume obtained in the control group (PBS-treated mice). The means±SEM (plus each individual data point) are represented. (C) Single growth curves of 67NR tumors treated with mono (anti-PD-1 antibody (n=10), RANK-Fc (n=10), GCG (n=10)) or combination therapy (anti-PD-1 plus RANK-Fc (n=10) or GCG (n=10)). Unlike RANKL inhibitors which have always been well tolerated, it is important to note that the third injection of anti-PD-1 antibody induced 50% mortality in tumor-bearing mice. P values were determined using one-way ANOVA followed by Bonferroni multiple comparison post hoc test (B). ANOVA, analysis of variance; GCG, gallocatechin gallate; i.p., intraperitoneal; PBS, phosphate-buffered saline; PD-1, programmed cell death protein-1; RANKL, receptor activator of nuclear factor κB ligand; TNBC, triple-negative breast cancer.

cells. Indeed, when DC/pDC were incubated with RANKL for 72 hours and then stimulated for maturation (LPS (DC) or CpG ODN (pDC) during 24 hours), we clearly observed that all cell surface maturation markers studied (CD80, CD83, CD86 and major histocompatibility complex (MHC) class I/II) were significantly downregulated when compared with LPS/CpG ODN-stimulated (control) cells. Interestingly, higher expressions of the inhibitory proteins ILT3 (DC) and ICOSL (pDC) as well as CCR7 (crucial for homing and cell trafficking to lymph nodes) were also detected in the case of preincubation with RANKL. In parallel, DC-CD4$^+$ T cell co-cultures were performed and we showed that DC exposed to RANKL promotes Treg cell differentiation and suppressive function, as demonstrated by the increased expression of Foxp3, CD25, CD69, Helios and Neuropilin-1 by lymphocytes (figure 7D) and the ability of these latter T cells (originally primed by DC pretreated with RANKL) to significantly reduce the proliferation of other allogeneic CD4$^+$ lymphocytes (figure 7E). Finally, the secretion profiles of DC preincubated or not with RANKL (before LPS stimulation) were assessed by cytokine array and, importantly, several proinflammatory cytokines (eg, IL-6, IL-16) and chemokines (eg, CCL5, CXCL10, MIF) pivotal for DC function have been shown to be drastically reduced (by up to 60%) in

RANKL-pretreated DC, further supporting the acquisition of a tolerogenic functionality in the presence of this ligand (figure 7F). Given the pleiotropic roles played by mTOR in innate immune cell regulation (for a review, see study by Weichhart et al[52]), we decided to evaluate whether an alteration of this signaling pathway could explain the RANKL-related defective DC maturation. As shown in figure 7G, the phosphorylation level of mTOR, p70 S6 kinase and S6 ribosomal protein was markedly reduced following a prolonged exposure (>48 hour) to RANKL. In accordance with the downregulation of mTOR signaling, a decreased phosphorylation of PI3K, Akt and TSC2, along with an increased expression of the negative regulator TSC1, were detected in DC cultured in the presence of RANKL for 48–72 hour (online supplemental figure 11). In order to confirm the key role played by mTOR inhibition in the tolerogenic commitment of antigen-presenting cells, both DC and pDC were incubated with Rapamycin (well-known mTORC1 inhibitor) or Torkinib/PP242 (potent mTORC1/2 inhibitor) for 2 hours before being stimulated for maturation with LPS (DC) or CpG ODN (pDC). Remarkably, collected results (reduced expression of maturation markers (CD80, CD83, CD86 and MHC class I/II) accompanied by an upregulation of CCR7 compared with LPS/CpG ODN-stimulated (control) cells) closely mimicked those
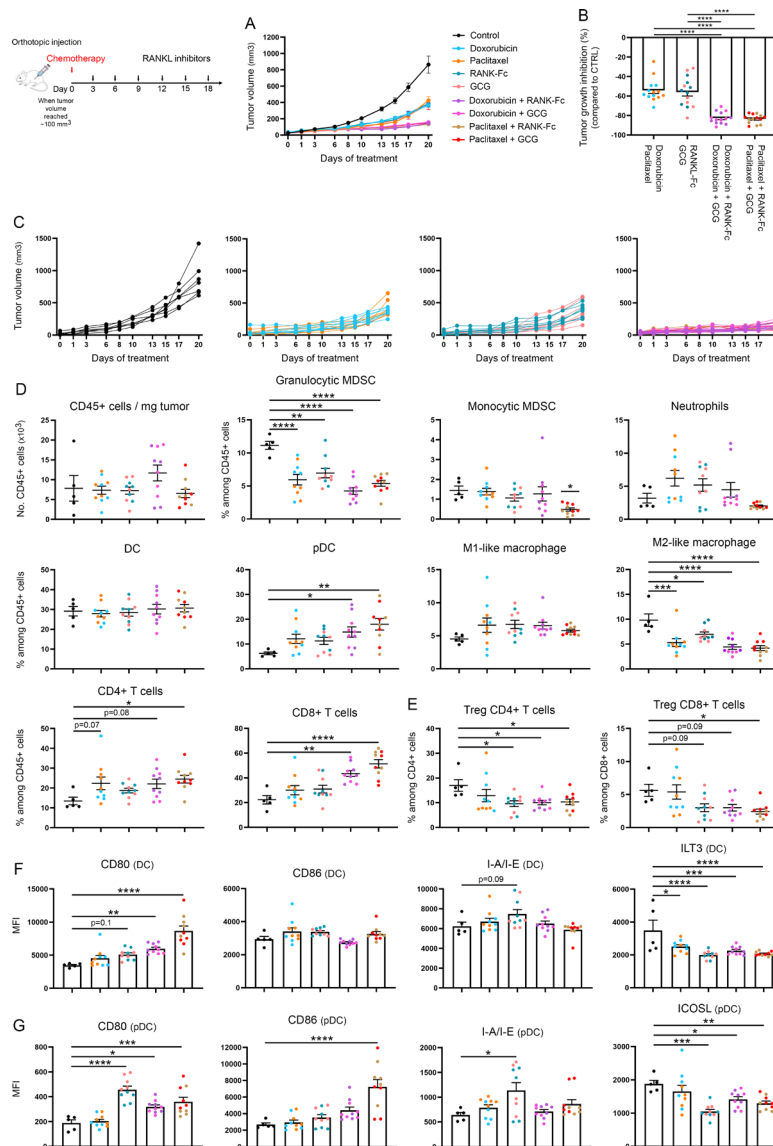
Figure 6 Combination of doxorubicin or paclitaxel-based chemotherapy with RANKL inhibitors displays substantial anticancer efficacy. (A) Mouse TNBC 67NR cells were orthotopically injected into the mammary fat pad of immunocompetent BALB/c mice. Tumor-bearing mice were treated with one single dose of chemotherapy (doxorubicin (2.5 mg/kg) or paclitaxel (10 mg/kg)), with RANKL inhibitors (RANK-Fc (1 mg/kg) and GCG (10 mg/kg), treatment at 3-day intervals) or with the combined treatment regimen. PBS-treated mice were used as controls. The mean tumor volumes±SEM are represented. (B) The tumor growth inhibition induced by doxorubicin, paclitaxel, RANK-Fc or GCG alone as well as by the combination regimens was determined. To do so, the volume of each harvested tumor was compared with the average tumor volume obtained in the control group. The means±SEM (plus each individual data point) are represented. (C) Single growth curves of 67NR tumors treated with mono or combination therapy. (D) Following mouse euthanasia, tumors were retrieved and enzymatically dissociated before flow cytometry analysis. Scatter dot plots showing the total number of (CD45$^+$) immune cells per milligram of tumor as well as the percentage of each individual immune cell population (neutrophils, granulocytic and monocytic MDSC, DC, pDC, M1-like and M2-like macrophages, CD4$^+$ and CD8$^+$ T cells) among CD45$^+$ cells in the different treated groups. The increased proportion of CD4$^+$/CD8$^+$ T lymphocytes (associated with the reduction of both granulocytic MDSC and M2-like macrophages) following chemotherapy should be noticed. The tumor-infiltrating immune cells were analyzed in 5 mice per condition. (E) Scatter dot plots illustrating the percentage of intratumor CD4$^+$ and CD8$^+$ Treg cells among total CD4$^+$ and CD8$^+$ populations in the different treatment groups. The activation status of DC (F) and pDC (G) was determined by analyzing the expression of several surface markers (CD80, CD86, I-A/I-E, ILT3 (DC) and ICOSL (pDC)) by flow cytometry. Data represent the mean fluorescent intensity (MFI)±SEM of 5 independent analyzes in each group (each individual data point is shown). Regardless of neoadjuvant chemotherapy, reduced proportions of CD4$^+$/CD8$^+$ Treg cells associated with increased activation of antigen-presenting cells were observed following RANKL blockade. Asterisks indicate statistically significant differences (*p<0.05; **p<0.01; ***p<0.001; ****p<0.0001). P values were determined using one-way ANOVA followed by Dunnett's multiple comparison post hoc test (D, E, F, G) or Bonferroni post-test (B). ANOVA, analysis of variance; DC, dendritic cell; GCG, gallocatechin gallate; MDSC, myeloid-derived suppressor cell; PBS, phosphate-buffered saline; pDC, plasmacytoid dendritic cell; RANKL, receptor activator of nuclear factor κB ligand; TNBC, triple-negative breast cancer; Treg, T regulatory.
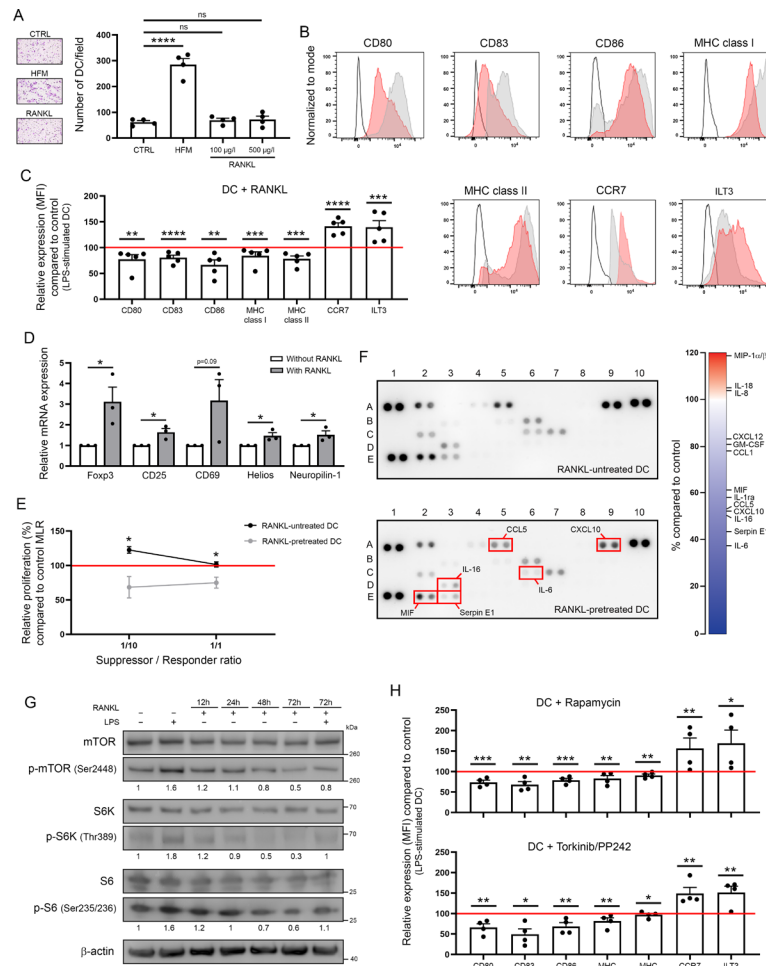
Figure 7 RANKL promotes the acquisition of a tolerogenic functionality by dendritic cells. (A) Influence of RANKL on DC migration in a Boyden chamber assay. Two different concentrations (100 and 500 µg/L) were tested. Data represent the means±SEM of four independent experiments performed in sextuplicate. (B) Representative FACS histograms showing the expression (normalized mean fluorescent intensity (MFI)) of CD80, CD83, CD86, MHC class I (HLA-ABC), MHC class II (HLA-DR), CCR7 and ILT3 on cell surface of DC cultured in the presence (red) or absence (gray) of 0.5 µg/mL RANKL during 3 days before LPS stimulation. Overlays were created using FlowJo software (V.10). (C) Expression of the aforementioned cell-surface molecules on DC pretreated with RANKL before stimulation with LPS. All data were normalized to LPS-stimulated DC (red line). Data represent the relative MFI±SEM of five independent experiments (each individual data point is shown). The significant reduction of all DC maturation markers studied (associated with the increased expression of both CCR7 and ILT3) in the case of RANKL exposure should be noticed. (D) CD4^{+} T cells were mixed with DC that were either pretreated with RANKL for 72 hours or not. After 6 days of co-culture, the expression of various immune tolerance markers (Foxp3, CD25, CD69, Helios, neuropilin-1) by T lymphocytes was determined by RT-qPCR. Results represent the means±SEM of three independent experiments performed in duplicate. (E) Suppressor activity of T cells originally primed by DC pretreated or not with RANKL. Allogeneic CD4^{+} T cells were co-cultured during 6 days with DC, either pretreated with RANKL or not. Cell mixture from the first mixed lymphocyte reaction (considered as potential "suppressor" cells) was then mixed with both freshly isolated T cells and other DC. Cell viability/proliferation was finally evaluated by MTT assay. Data represent the means±SEM of four independent experiments. (F) Cytokines/chemokines secreted by RANKL-untreated DC and DC pretreated with RANKL were detected using cytokine array. The respective MIF, CCL5, CXCL10, IL-16, Serpin E1 and IL-6 spots are highlighted (red boxes). The reduced secretions of these proinflammatory or pivotal molecules for DC functionality should be noticed. (G) Phosphorylation status of mTOR, S6 kinase and S6 ribosomal protein was determined by Western blot in DC exposed or not to RANKL. A representative immunoblot from three independent experiments is shown. The protein bands were quantified by densitometric analysis (ImageJ software). (H) Expression of maturation markers (CD80, CD83, CD86 and MHC class I/II) as well as CCR7 and ILT3 on DC pretreated with a mTOR inhibitor (Rapamycin or Torkinib/PP242) before being stimulated with LPS. All data were normalized to LPS-stimulated DC (red line). Data represent the relative MFI±SEM of four independent experiments (each individual data point is shown). The similarity between these latter results and those obtained with DC exposed to RANKL for 72 hours should be noticed. Asterisks indicate statistically significant differences (*$p<0.05$; **$p<0.01$; ***$p<0.001$; ****$p<0.0001$). P values were determined using one-way ANOVA followed by Dunnett's multiple comparison post hoc test (A), one sample t-test (C, D, H) or unpaired t-test (E). ANOVA, analysis of variance; DC, dendritic cell; FACS, fluorescence-activated cell sorting; HFM, human fibroblast conditioned medium; LPS, lipopolysaccharide; MHC, major histocompatibility complex; mRNA, messenger RNA; ns, not significant; RANKL, receptor activator of nuclear factor κB ligand; RT-qPCR, quantitative reverse transcription PCR.

obtained with DC/pDC exposed to RANKL (figure 7H and online supplemental figure 10D).

DISCUSSION

Originally discovered for its regulatory function in bone formation, data accumulated during the last two decades have clearly established that the RANKL/RANK axis acts well beyond the bone field. Although not fully understood/characterized and still the subject of various (pre) clinical investigations, numerous studies notably demonstrated the contribution of soluble RANKL in cancer development and spread (especially bone metastasis). Indeed, this multifunctional ligand has been shown to induce cell proliferation, cancer cell motility and invasiveness by promoting epithelial–mesenchymal transition and by acting as a chemotactic factor to attract the malignant cells to bones.[9 53–55] It is however important to mention that the studies available in the literature have almost exclusively focused their attention on the direct effect of RANKL on epithelial tumor cells while, interestingly, single-cell transcriptomic data highlighted that other cell types (eg, endothelial, mesenchymal and immune cells) present within the tumor microenvironment also express the receptor RANK (and could, therefore, be influenced by the RANKL/RANK system as well). Supporting this hypothesis, more than half of the Top 10 GO biological process gene sets enriched positively in RANKL[high]-expressing TNBC were related to immune regulation/differentiation. In the specific context of breast malignancies not expressing hormone (estrogen and progesterone) receptors and HER2, remarkably, high RANKL expression was also associated with better clinical outcomes. These results mimic those reported with PD-L1, another targetable immunotherapeutic protein which is also an independent predictor of favorable survival in patients with TNBC (for a meta-analysis, see study by Matikas et al[56]). Although the positive prognostic value of an immunosuppressive molecule may, at first glance, seem counterintuitive, accumulating evidence supports that tumors with preexisting immunity (even with high proportions of tolerogenic cells) respond better to treatments (eg, chemoradiotherapy, immune checkpoint-based immunotherapy) than their immunologically ignorant counterparts (also called immune deserts). In the present case, the correlation between RANKL positivity and the densities of both Foxp3^{+} (Treg) and CD206^{+} (M2-like macrophages) cells in primary TNBC, the numerous immune-associated signatures enriched in RANKL^{high}-expressing tumors as well as the favorable prognosis displayed by these tumors clearly support this theory.

After having evidenced that TNBC was an appropriate tumor (sub)type to analyze the potential therapeutic efficacy of RANKL blockade, in vivo assays were performed. Despite the intrinsic variations (relatively modest in the present case) inherent in animal experiments, strikingly, an inhibition of tumor growth was reproducibly detected in each syngeneic mouse model (4T1, 67NR, E0771) after a latency period of 5–7 days following the first injection, most likely corresponding to the required time for the adaptive immunity to be remobilized. In agreement with this assumption, the dependence on the adaptive immune system was noticeably illustrated by the absence of anticancer effect in vitro as well as when immunocompromised mice were used. In contrast to data recently published,[57] our results do not argue for a marked direct impact of RANKL inhibition on tumor cell growth/ behavior. This discordance could easily be explained by differences in terms of RANK expression level. Indeed, the patient-derived orthoxenografts used by Ciscar et al strongly expressed the receptor RANK whereas our mouse models displayed moderate (67NR) or low (4T1, E0771) RANK immunoreactivity. Altogether, the intensity of anti-RANK immunoreactivity displayed by tumor cells does not appear to be an accurate predictive biomarker of RANKL blockade efficacy. In the light of our results, the density of tumor-infiltrating immune cells (especially DC/pDC and T cells) could be regarded as an interesting alternative predictor of patients' response and would definitely deserve to be determined in ongoing clinical trials using Denosumab in monotherapy or in combination.

Without modifying the global number of CD45^{+} cells infiltrating the tumor microenvironment (supported, in particular, by the absence of chemotactic activity of RANKL on antigen-presenting cells), we showed that RANKL blockade alone induces a significant remodeling of the tumor immune landscape characterized by an increased activation of DC/pDC and a subsequent drastic reduction of Treg cells (by up to 70%). Through antibody-mediated depletion experiments, we confirmed the crucial involvement of this loss of Treg cells in the antitumor immunotherapeutic effect of RANKL inhibitors. The immunosuppressive action of RANKL was further confirmed in vitro by the impaired maturation and function exhibited by antigen-presenting cells incubated with recombinant RANKL before LPS (DC) or CpG ODN (pDC) stimulation. Expressing low levels of CD80, CD83, CD86, MHC class I/II and displaying an altered secretion profile, these cells reduced T cell proliferation and stimulated the differentiation of naive CD4^{+} T lymphocytes into Treg cells. As previously described,[58 59] the high expression of inhibitory proteins ILT3 (DC) and ICOSL (pDC) following RANKL incubation could be critical in this DC/pDC-mediated Treg induction. Interestingly, the expression of CCR7 on the cell surface of DC/pDC was also significantly upregulated after incubation with RANKL, suggesting that antigen-presenting cells that have been exposed to this ligand increase their capacity to migrate to tumor-draining lymph nodes. However, their altered (semimature) phenotype prevents them from appropriately stimulating anticancer immune responses. Mechanistically, we demonstrated that RANKL-induced acquisition of tolerogenic functionality by DC/pDC was dependent on inhibition of the

mTOR pathway. This downregulation of mTOR most certainly also explains the strong negative enrichment of genes involved in mitochondrial function detected in RANKL[high]-expressing neoplasms. Last but not least, it is interesting to mention that RANKL-dependent inhibition of mTOR signaling not only alters the functionality of antigen-presenting cells, but has also been found to actively participate in osteoclast differentiation.[60 61]

Beside the beneficial effect on primary (pre-existing) neoplasms, a reduced metastatic dissemination to lungs of TNBC cells was also observed following pharmacological blockade of RANKL. While effective inhibition of de novo bone metastasis formation has been extensively characterized in various cancer models, the ability of RANKL inhibitors to block distant metastasis to non-skeletal sites is much less well defined. Using a spontaneous mouse mammary tumor model (MMTV-neu transgenic mice), it is interesting to mention that two separate groups have also previously reported a significant decrease in lung metastatic foci upon inhibition of the RANKL/RANK axis.[62 63] Whether this antimetastatic function of RANKL inhibitors is linked to a direct effect on circulating tumor cells, to a remodeling of premetastatic niche and/or to an activation of the adaptive immune system in blood/distant organs (similarly to what we highlighted here in primary tumors) remains unclear but would certainly deserve specific preclinical investigations.

Combining immunomodulators with each other or with chemotherapeutic molecules represents a new trend in patients' with cancer treatment. One of the best examples is undoubtedly the combination therapy using PD-1 and CTLA-4 inhibitors which has been recently approved for the first-line treatment of various neoplasms (eg, non-small cell lung cancer, mesothelioma, advanced renal cell carcinoma). Here, we tested the concomitant blockade of RANKL and PD-1 but, despite reported anticancer efficacy as monotherapy, an absence of additive or synergistic effects was reported. These observations could be explained by a common/close mechanism of action underlying successful anti-RANKL and anti-PD-1 cancer immunotherapy. Indeed, similar to what we showed in the present study with RANKL blockade, the full activation of tumor-infiltrating T cells by anti-PD-1 antibody has also been shown to be indirect and requires efficient crosstalk between T lymphocytes and antigen-presenting cells.[64] Furthermore, the mTOR pathway is critical to T cell and DC/pDC functions and is targeted by both RANKL/RANK axis and PD-1 signaling.[65 66] Given these similarities, any additive effects of cumulative RANKL and PD-1 inhibition seem, therefore, highly unlikely. Despite the negative results reported with anti-PD-1 immunotherapy, this does not, of course, rule out the possibility that combining RANKL blockade with another checkpoint inhibitor (eg, Fc-active CTLA-4 or LAG-3 monoclonal antibody) could have an additive effect, warranting further specific preclinical investigations. The timing of treatments would also merit being explored in more detail as it remains a subject of intense debate in translational/clinical oncology and could notably help explain the mixed results reported in the literature regarding treatment regimens involving drugs targeting the PI3K/Akt/mTOR pathway in combination with chemo/immunotherapy.[67] Indeed, PD-1 blockade has recently been shown to work after cessation of mTOR inhibition, whereas simultaneous treatment proved ineffective.[68] Alongside the combination with immune checkpoint inhibition, the efficacy of neoadjuvant chemotherapy plus RANKL blockade was also evaluated. Interestingly, while maintaining the antimetastatic effect of pharmacological RANKL inhibitors, a greater primary tumor growth inhibition was detected compared with each individual treatment. This beneficial effect is very likely explained by the expected (and observed) increase of tumor-infiltrating effector T cells. Indeed, through various (in)direct mechanisms (eg, the release of tumor-specific antigens from dying cells), the administration of chemotherapeutic agents primes T cell-dependent immune responses, which ultimately results in an enhanced response to immune blockers.[69 70] Therefore, such a combination strategy should be favored in future clinical trials. Furthermore, as shown here at both mRNA and protein levels, not all tumors moderately/highly express RANKL, highlighting that, unlike what has been done so far (eg, NCT01077154 and NCT02129699), a more comprehensive characterization of enrolled patients, particularly regarding their immune cell infiltration profiles, appears essential to accurately identify those who are most likely to benefit from RANKL blockade.

ORCID iDs
Pascale Hubert http://orcid.org/0000-0002-0799-3047
Michael Herfs http://orcid.org/0000-0002-4382-8997

REFERENCES

1 Wong BR, Josien R, Lee SY, *et al*. TRANCE (tumor necrosis factor [TNF]-related activation-induced cytokine), a new TNF family member predominantly expressed in T cells, is a dendritic cell-specific survival factor. *J Exp Med* 1997;186:2075–80.
2 Anderson DM, Maraskovsky E, Billingsley WL, *et al*. A homologue of the TNF receptor and its ligand enhance T-cell growth and dendritic-cell function. *Nature New Biol* 1997;390:175–9.
3 Yasuda H, Shima N, Nakagawa N, *et al*. Osteoclast differentiation factor is a ligand for osteoprotegerin/osteoclastogenesis-inhibitory factor and is identical to TRANCE/RANKL. *Proc Natl Acad Sci U S A* 1998;95:3597–602.
4 Lacey DL, Timms E, Tan HL, *et al*. Osteoprotegerin ligand is a cytokine that regulates osteoclast differentiation and activation. *Cell* 1998;93:165–76.
5 Proposed Standard Nomenclature for New Tumor Necrosis Factor Family Members Involved in the Regulation of Bone Resorption. *J Bone Miner Res* 2000;15:2293–6.
6 Ono T, Hayashi M, Sasaki F, *et al*. RANKL biology: bone metabolism, the immune system, and beyond. *Inflamm Regen* 2020;40:2.
7 Fata JE, Kong YY, Li J, *et al*. The osteoclast differentiation factor osteoprotegerin-ligand is essential for mammary gland development. *Cell* 2000;103:41–50.
8 Kong YY, Yoshida H, Sarosi I, *et al*. OPGL is a key regulator of osteoclastogenesis, lymphocyte development and lymph-node organogenesis. *Nature New Biol* 1999;397:315–23.
9 Palafox M, Ferrer I, Pellegrini P, *et al*. RANK induces epithelial-mesenchymal transition and stemness in human mammary epithelial cells and promotes tumorigenesis and metastasis. *Cancer Res* 2012;72:2879–88.
10 Fujimura T, Kambayashi Y, Furudate S, *et al*. Receptor Activator of NF-κB Ligand Promotes the Production of CCL17 from RANK+ M2 Macrophages. *J Invest Dermatol* 2015;135:2884–7.
11 Coleman R, Finkelstein DM, Barrios C, *et al*. Adjuvant denosumab in early breast cancer (D-CARE): an international, multicentre, randomised, controlled, phase 3 trial. *Lancet Oncol* 2020;21:60–72.
12 Peters S, Danson S, Hasan B, *et al*. A Randomized Open-Label Phase III Trial Evaluating the Addition of Denosumab to Standard First-Line Treatment in Advanced NSCLC: The European Thoracic Oncology Platform (ETOP) and European Organisation for Research and Treatment of Cancer (EORTC) SPLENDOUR Trial. *J Thorac Oncol* 2020;15:1647–56.
13 Arnold M, Morgan E, Rumgay H, *et al*. Current and future burden of breast cancer: Global statistics for 2020 and 2040. *Breast* 2022;66:15–23.
14 Perou CM, Sørlie T, Eisen MB, *et al*. Molecular portraits of human breast tumours. *Nature New Biol* 2000;406:747–52.
15 Sørlie T, Perou CM, Tibshirani R, *et al*. Gene expression patterns of breast carcinomas distinguish tumor subclasses with clinical implications. *Proc Natl Acad Sci USA* 2001;98:10869–74.
16 Vasconcelos I, Hussainzada A, Berger S, *et al*. The St. Gallen surrogate classification for breast cancer subtypes successfully predicts tumor presenting features, nodal involvement, recurrence patterns and disease free survival. *Breast* 2016;29:181–5.
17 Jiang Y-Z, Ma D, Suo C, *et al*. Genomic and Transcriptomic Landscape of Triple-Negative Breast Cancers: Subtypes and Treatment Strategies. *Cancer Cell* 2019;35:428–40.
18 Lehmann BD, Bauer JA, Chen X, *et al*. Identification of human triple-negative breast cancer subtypes and preclinical models for selection of targeted therapies. *J Clin Invest* 2011;121:2750–67.
19 Burstein MD, Tsimelzon A, Poage GM, *et al*. Comprehensive genomic analysis identifies novel subtypes and targets of triple-negative breast cancer. *Clin Cancer Res* 2015;21:1688–98.
20 Tutt ANJ, Garber JE, Kaufman B, *et al*. Adjuvant Olaparib for Patients with BRCA1- or BRCA2-Mutated Breast Cancer. *N Engl J Med* 2021;384:2394–405.
21 Cortes J, Rugo HS, Cescon DW, *et al*. Pembrolizumab plus Chemotherapy in Advanced Triple-Negative Breast Cancer. *N Engl J Med* 2022;387:217–26.
22 Schmid P, Adams S, Rugo HS, *et al*. Atezolizumab and Nab-Paclitaxel in Advanced Triple-Negative Breast Cancer. *N Engl J Med* 2018;379:2108–21.
23 Demoulin S, Roncarati P, Delvenne P, *et al*. Production of large numbers of plasmacytoid dendritic cells with functional activities from CD34(+) hematopoietic progenitor cells: use of interleukin-3. *Exp Hematol* 2012;40:268–78.
24 Hubert P, Herman L, Roncarati P, *et al*. Altered α-defensin 5 expression in cervical squamocolumnar junction: implication in the formation of a viral/tumour-permissive microenvironment. *J Pathol* 2014;234:464–77.
25 Hubert P, Roncarati P, Demoulin S, *et al*. Extracellular HMGB1 blockade inhibits tumor growth through profoundly remodeling immune microenvironment and enhances checkpoint inhibitor-based immunotherapy. *J Immunother Cancer* 2021;9:e001966.
26 Cheng J, Zheng J, Guo N, *et al*. I-BET151 inhibits osteoclastogenesis via the RANKL signaling pathway in RAW264.7 macrophages. *Mol Med Rep* 2017;16:8406–12.
27 Xu H, Yin D, Liu T, *et al*. Tea polysaccharide inhibits RANKL-induced osteoclastogenesis in RAW264.7 cells and ameliorates ovariectomy-induced osteoporosis in rats. *Biomed Pharmacother* 2018;102:539–48.
28 Chevalier C, Çolakoğlu M, Brun J, *et al*. Primary mouse osteoblast and osteoclast culturing and analysis. *STAR Protoc* 2021;2:100452.
29 Bankhead P, Loughrey MB, Fernández JA, *et al*. QuPath: Open source software for digital pathology image analysis. *Sci Rep* 2017;7:16878.
30 Gao J, Aksoy BA, Dogrusoz U, *et al*. Integrative analysis of complex cancer genomics and clinical profiles using the cBioPortal. *Sci Signal* 2013;6:pl1.
31 Cerami E, Gao J, Dogrusoz U, *et al*. The cBio cancer genomics portal: an open platform for exploring multidimensional cancer genomics data. *Cancer Discov* 2012;2:401–4.
32 Wu T, Hu E, Xu S, *et al*. clusterProfiler 4.0: A universal enrichment tool for interpreting omics data. *The Innovation* 2021;2:100141.
33 Yu G, Wang L-G, Han Y, *et al*. clusterProfiler: an R package for comparing biological themes among gene clusters. *OMICS* 2012;16:284–7.
34 Bruyere D, Monnien F, Colpart P, *et al*. Treatment algorithm and prognostic factors for patients with stage I-III carcinoma of the anal canal: a 20-year multicenter study. *Mod Pathol* 2021;34:116–30.
35 Herfs M, Roncarati P, Koopmansch B, *et al*. A dualistic model of primary anal canal adenocarcinoma with distinct cellular origins, etiologies, inflammatory microenvironments and mutational signatures: implications for personalised medicine. *Br J Cancer* 2018;118:1302–12.
36 Bruyere D, Roncarati P, Lebeau A, *et al*. Human papillomavirus E6/E7 oncoproteins promote radiotherapy-mediated tumor suppression by globally hijacking host DNA damage repair. *Theranostics* 2023;13:1130–49.
37 Taylor AM, Shih J, Ha G, *et al*. Genomic and Functional Approaches to Understanding Cancer Aneuploidy. *Cancer Cell* 2018;33:676–89.
38 Buffa FM, Harris AL, West CM, *et al*. Large meta-analysis of multiple cancers reveals a common, compact and highly prognostic hypoxia metagene. *Br J Cancer* 2010;102:428–35.
39 Sordillo EM, Pearse RN. RANK-Fc: a therapeutic antagonist for RANK-L in myeloma. *Cancer* 2003;97:802–12.
40 Hur J, Ghosh A, Kim K, *et al*. Design of a RANK-Mimetic Peptide Inhibitor of Osteoclastogenesis with Enhanced RANKL-Binding Affinity. *Mol Cells* 2016;39:316–21.
41 Melagraki G, Ntougkos E, Papadopoulou D, *et al*. *In Silico* Discovery of Plant-Origin Natural Product Inhibitors of Tumor Necrosis Factor

(TNF) and Receptor Activator of NF-κB Ligand (RANKL). *Front Pharmacol* 2018;9:800.

42 Xu H, Liu T, Li J, *et al*. Oxidation derivative of (-)-epigallocatechin-3-gallate (EGCG) inhibits RANKL-induced osteoclastogenesis by suppressing RANK signaling pathways in RAW 264.7 cells. *Biomed Pharmacother* 2019;118:109237.

43 Jeong S, Lee S, Kim K, *et al*. Isoliquiritigenin Derivatives Inhibit RANKL-Induced Osteoclastogenesis by Regulating p38 and NF-κB Activation in RAW 264.7 Cells. *Molecules* 2020;25:3908.

44 De Leon-Oliva D, Barrena-Blázquez S, Jiménez-Álvarez L, *et al*. The RANK-RANKL-OPG System: A Multifaceted Regulator of Homeostasis, Immunity, and Cancer. *Medicina (Kaunas)* 2023;59:1752.

45 Emery JG, McDonnell P, Burke MB, *et al*. Osteoprotegerin is a receptor for the cytotoxic ligand TRAIL. *J Biol Chem* 1998;273:14363–7.

46 Takeda K, Smyth MJ, Cretney E, *et al*. Critical role for tumor necrosis factor-related apoptosis-inducing ligand in immune surveillance against tumor development. *J Exp Med* 2002;195:161–9.

47 Sag D, Ayyildiz ZO, Gunalp S, *et al*. The Role of TRAIL/DRs in the Modulation of Immune Cells and Responses. *Cancers (Basel)* 2019;11:1469.

48 Rupp T, Genest L, Babin D, *et al*. Anti-CTLA-4 and anti-PD-1 immunotherapies repress tumor progression in preclinical breast and colon model with independent regulatory T cells response. *Transl Oncol* 2022;20:101405.

49 Brockwell NK, Owen KL, Zanker D, *et al*. Neoadjuvant Interferons: Critical for Effective PD-1-Based Immunotherapy in TNBC. *Cancer Immunol Res* 2017;5:871–84.

50 Mall C, Sckisel GD, Proia DA, *et al*. Repeated PD-1/PD-L1 monoclonal antibody administration induces fatal xenogeneic hypersensitivity reactions in a murine model of breast cancer. *Oncoimmunology* 2016;5:e1075114.

51 Sordo-Bahamonde C, Lorenzo-Herrero S, Gonzalez-Rodriguez AP, *et al*. Chemo-Immunotherapy: A New Trend in Cancer Treatment. *Cancers (Basel)* 2023;15:2912.

52 Weichhart T, Hengstschläger M, Linke M. Regulation of innate immune cell function by mTOR. *Nat Rev Immunol* 2015;15:599–614.

53 Jones DH, Nakashima T, Sanchez OH, *et al*. Regulation of cancer cell migration and bone metastasis by RANKL. *Nature New Biol* 2006;440:692–6.

54 Sigl V, Owusu-Boaitey K, Joshi PA, *et al*. RANKL/RANK control Brca1 mutation- . *Cell Res* 2016;26:761–74.

55 Okamoto K. Role of RANKL in cancer development and metastasis. *J Bone Miner Metab* 2021;39:71–81.

56 Matikas A, Zerdes I, Lövrot J, *et al*. Prognostic Implications of PD-L1 Expression in Breast Cancer: Systematic Review and Meta-analysis of Immunohistochemistry and Pooled Analysis of Transcriptomic Data. *Clin Cancer Res* 2019;25:5717–26.

57 Ciscar M, Trinidad EM, Perez-Chacon G, *et al*. RANK is a poor prognosis marker and a therapeutic target in ER-negative postmenopausal breast cancer. *EMBO Mol Med* 2023;15:e16715.

58 Vlad G, Suciu-Foca N. Induction of antigen-specific human T suppressor cells by membrane and soluble ILT3. *Exp Mol Pathol* 2012;93:294–301.

59 Lee H-J, Kim S-N, Jeon M-S, *et al*. ICOSL expression in human bone marrow-derived mesenchymal stem cells promotes induction of regulatory T cells. *Sci Rep* 2017;7:44486.

60 Huynh H, Wan Y. mTORC1 impedes osteoclast differentiation via calcineurin and NFATc1. *Commun Biol* 2018;1:29.

61 Hiraiwa M, Ozaki K, Yamada T, *et al*. mTORC1 Activation in Osteoclasts Prevents Bone Loss in a Mouse Model of Osteoporosis. *Front Pharmacol* 2019;10:684.

62 Gonzalez-Suarez E, Jacob AP, Jones J, *et al*. RANK ligand mediates progestin-induced mammary epithelial proliferation and carcinogenesis. *Nature New Biol* 2010;468:103–7.

63 Tan W, Zhang W, Strasner A, *et al*. Tumour-infiltrating regulatory T cells stimulate mammary cancer metastasis through RANKL-RANK signalling. *Nature New Biol* 2011;470:548–53.

64 Garris CS, Arlauckas SP, Kohler RH, *et al*. Successful Anti-PD-1 Cancer Immunotherapy Requires T Cell-Dendritic Cell Crosstalk Involving the Cytokines IFN-γ and IL-12. *Immunity* 2018;49:1148–61.

65 Chi H. Regulation and function of mTOR signalling in T cell fate decisions. *Nat Rev Immunol* 2012;12:325–38.

66 Quan Z, Yang Y, Zheng H, *et al*. Clinical implications of the interaction between PD-1/PD-L1 and PI3K/AKT/mTOR pathway in progression and treatment of non-small cell lung cancer. *J Cancer* 2022;13:3434–43.

67 Costa RLB, Han HS, Gradishar WJ. Targeting the PI3K/AKT/mTOR pathway in triple-negative breast cancer: a review. *Breast Cancer Res Treat* 2018;169:397–406.

68 Ando S, Perkins CM, Sajiki Y, *et al*. mTOR regulates T cell exhaustion and PD-1-targeted immunotherapy response during chronic viral infection. *J Clin Invest* 2023;133:e160025.

69 Liu J, Blake SJ, Yong MCR, *et al*. Improved Efficacy of Neoadjuvant Compared to Adjuvant Immunotherapy to Eradicate Metastatic Disease. *Cancer Discov* 2016;6:1382–99.

70 O'Donnell JS, Hoefsmit EP, Smyth MJ, *et al*. The Promise of Neoadjuvant Immunotherapy and Surgery for Cancer Treatment. *Clin Cancer Res* 2019;25:5743–51.